Christoph Heininger, BSc

Monoglyceride lipase activity influences growth and phosphoprotein profile of lung cancer cells

MASTER'S THESIS

to achieve the university degree of

Master of Science

Master's degree programme:

Biochemistry and Molecular Biomedicine

submitted to

Graz University of Technology

Supervisor

Univ. Prof. Dipl.-Ing. Dr. techn. Ruth Birner-Grünberger

Diagnostic and Research Institute of Pathology, Medical University of Graz

Research Unit "Functional Proteomics and Metabolic Pathways

Graz, September 2020

AFFIDAVIT

I declare that I have authored this thesis independently, that I have not used other than the declared sources/resources, and that I have explicitly indicated all material which has been quoted either literally or by content from the sources used. The text document uploaded to TUGRAZonline is identical to the present master's thesis.

Date, Signature

Acknowledgements

First and foremost, I want to thank Prof. Ruth Birner-Grünberger for giving me the opportunity to work in her lab as part of the team that call themselves the “Proteomics Pirates”. As the “Captain” of this pirate crew, Prof. Birner-Grünberger acts as a wise and trustworthy leader without being dictatorial toward her crew. She is also greatly empathetic and enormously friendly with everyone who has the pleasure of working with her. For all those reasons, I appreciate the time I spent in her lab/crew. Thank you, Ruth, for everything!

Secondly, my thanks go to Tamara Tomin. She is the “Second Mate” of the “Proteomics Pirates”. What she lacks in experience when compared to the “Captain”, she makes up for with sheer talent. You could say, she is a naturally gifted scientist. She was the one to introduce me into the practical laboratory work and was always happy to answer any questions coming her way. By virtue of her amicable and outgoing character I not only value Tamara for the professional guidance, but also as a friend. I will always be grateful to you, Tamara, thank you!

If a crew has a “Captain” and a “Second Mate”, it must also have a “First Mate”. In this case, it is Matthias Schittmayer-Schantl. He is the “creative mastermind” of the crew, although some claim his ideas to be a little crazy sometimes. Nevertheless, he is a great scientist and good mate to enjoy some booze with. Thanks for everything, Matthias, including the whiskey!

A special salute goes to Petra Krenn, who had to deal with interpreting a similar phosphoproteomics experimental design. Interpretation of such data sometimes leaves oneself frustrated and unable to see the forest for the trees, however Petra never threw in the towel and despite having her own massive dataset to make sense of, she never hesitated to aid me in my phosphoproteomics endeavor. Petra, thank you for being a role model for resilience when working with seemingly endless data!

Jürgen Gindlhuber is the imaging specialist in the group. What role in a pirate crew could be equivalent to a microscopist in a lab? Something with exceptional vision. Maybe the lookout on the crow’s nest? Or the gunner? If you asked Jürgen, he would probably say, he can do both. At the same time. With only one microscope. While someone might find his claim to be able to do ANY experiment or analysis with the help of a microscope to be utterly ridiculous, one cannot deny, that his proficiency with imaging techniques is unparalleled in the group. Jürgen also tends to prioritize helping others with their issues over his own work, which everyone gets to appreciate from time to time. Thank you, Jürgen, for the invaluable help in regard to microscopy and image analysis!

I was not the only apprentice in the crew during my time. Sophie Honeder joined shortly after I did. She is a very quick learner and will undoubtably become a great scientist. Aside from her affinity for everything science, I appreciate her friendliness and outgoing nature most. Sophie, I will always fondly remember the talks and laughs we shared!

Of course, every pirate crew needs people that tend to the ship, that keep things running. This would be Laura Liesinger, Barbara Darnhofer and Stefan Spörk. They were tirelessly fixing machines when they were not running and took great care to keep them running when they did. Not only that, the three are also always more than happy to help with practical work in the lab. And if someone follows one of Laura's or Babsi's protocols for sample preparation, they are pretty much guaranteed to succeed. Thank you, Laura, Babsi and Stefan for all your efforts!

Also, I want to thank my family for always supporting me and having my back in good times and in not so good times. Special thanks go to my mother, who always let me choose my own path and being 100% supportive all the way. Thank you, mum!

One last "Thank you" goes to a very special person who has become very dear to me in the last few years. She has helped me through some tough times and kept pushing me to be a better version of myself. Thank you to that very special someone, you know who you are!

Table of contents

Abstract

Monoglyceride lipase (MGL) is an important enzyme acting in lipolysis, hydrolyzing monoglycerides into glycerol and free fatty acids. MGL is implicated to impact proliferation and proliferation-related pathways in various cancer types, including lung cancer. This thesis investigated the differences in lipid droplet content and expression of selected proteins in a panel of lung adenocarcinoma cell lines. I could show that chemical inhibition of MGL results in an increase in proliferation in H358 and H441 lung cancer cell lines. These cells' migratory abilities however remained unaltered. Phosphoproteomics analysis was employed to examine alterations in the degree and pattern of phosphorylation in H358 and H441 cells upon inhibition of MGL. Three different approaches to the data analysis independently hinted toward a modification of the Wnt pathway and thus a possible involvement of MGL in the regulation of said pathway. The results presented in this thesis support the hypothesis that MGL activity hinders cell growth in certain cancer cell lines and provides a potential signaling pathway MGL might be involved in, which could explain the observed discrepancy in proliferation.

Zusammenfassung

Monoacylglycerin Lipase (MGL) ist ein wichtiges Enzym in der Lipolyse, das Monoacylglycerine zu Glycerin und freien Fettsäuren hydrolysiert. MGL wird mit Proliferation und proliferations-beeinflussenden Signalwegen in verschiedenen Krebs-Arten, ebenso in Lungenkrebs, in Verbindung gebracht. Diese Masterarbeit untersuchte die Unterschiede in der Menge der Lipidtropfen und die Expression ausgewählter Proteine in einer Sammlung von Lungen-Adenokarzinom Zelllinien. Ich konnte zeigen, dass die chemische Inhibierung der MGL eine erhöhte Proliferation von H358 und H441 Lungenkrebs Zelllinien zur Folge hatte. Die migratorischen Fähigkeiten dieser Zellen blieben allerdings unverändert. Eine Phosphoproteomik-Analyse wurde angewandt, um Veränderungen im Auftreten von Phosphorylierungen in H358 und H441 Zellen zu untersuchen, wenn MGL inhibiert wird. Drei unterschiedliche Herangehensweisen der Datenanalyse deuteten unabhängig voneinander auf eine Anpassung des Wnt Signalweges und somit auf eine mögliche Involvierung der MGL in diesen Signalweg hin. Die in dieser Masterarbeit präsentierten Ergebnisse unterstützen die Hypothese, dass die Aktivität der MGL das Wachstum in bestimmten Krebs Zelllinien unterbindet und bietet womöglich eine Erklärung, in welchem Signalweg MGL agiert, was eine mögliche Begründung für die beobachteten Wachstumsunterschiede sein könnte.

Introduction &
Hypothesis and Aim

Recent numbers of the American Cancer Society solidify lung (& bronchus) cancer as one of the most occurring and most deadly malignancies in the USA (Siegel, Miller, and Jemal 2020). In terms of new cases, lung cancer was second in both male (13% of new cases) and female (12% of new cases) patients, following only prostate and breast cancer, respectively. In terms of mortality an estimated 23% of men died of lung cancer, with 22% of females having succumbed to this cancer. Therefore, lung cancer claims the highest number of cancer-related deaths per year. In Europe, the numbers paint a similar picture (Ferlay et al. 2018): In men around 15% of expected cancer cases in 2018 were lung cancer, only overtaken by prostate cancer, with almost one quarter of expected deaths attributed to lung cancer. In women, lung cancer ranks only third highest (8.5%) in terms of new cases, behind breast and colorectal cancer. Breast cancer claims the highest number of female patients' lives (16.2%), followed shortly, however, by lung cancer (14.2%).

Lung cancer and more specifically non-small cell lung cancer (NSCLC) can carry a variety of genetic mutations, altering tumor suppressor genes, proto-oncogenes and/or DNA repair genes. Among the more common and well understood mutations are those that affect the epidermal growth factor receptor (EGFR). This receptor tyrosine kinase can be either overexpressed or activated through mutations and EGFR itself then activates several signaling pathways, like the Phosphoinositide 3-kinase/Protein kinase B (PI3K/AKT) pathway or the Ras/mitogen-activated protein kinase (Ras/MAPK) (MAPK is henceforth called by its alternative name, ERK, for extracellular signal-regulated kinase) pathway (Sigismund, Avanzato, and Lanzetti 2018). Through these pathways, EGFR's effect on survival, proliferation and migratory abilities is facilitated. Both ERK (Vicent et al. 2004) and AKT (David et al. 2004) have been shown to be activated in NSCLC. Additionally, the intracellular tyrosine kinase SRC (pronounced "sarc", short for "sarcoma"), which also influences signaling pathways like the ERK and AKT pathways, has been implicated as a therapeutic target in NSCLC (Giaccone and Zucali 2008). It is widely known, that cancer cells undergo changes in their metabolism as one of the hallmarks of cancer. Switching glucose metabolism to aerobic glycolysis – known as the Warburg Effect – was already described in the 1920s (Warburg, Wind, and Negelein 1926). In recent years, a considerable amount of research went into understanding how lipid metabolism is changed in tumors. A "derailed cellular lipidome" in cancer contributes to cancer hallmarks, owing to the complexity of lipids and their various functions (Molendijk et al. 2020). The strategy of choice in cancer to meet their altered requirements in lipid metabolism is often increased uptake of exogenous lipids or an increase in de novo synthesis (Beloribi-Djefaflia, Vasseur, and Guillaumond 2016). Excess lipids are then stored in lipid droplets (LD), organelles

acting as storage compartments for neutral lipids like triacylglycerol (TAG) and cholesteryl esters (CEs). LDs contribute in several ways in meeting cancer hallmarks (Cruz et al. 2020). The breakdown of TAGs by adipose triglyceride lipase (ATGL), hormone sensitive lipase (HSL) and monoacylglycerol lipase (MGL) is known as lipolysis (Knapp and Gorski 2017). Every one of those enzymes hydrolyses one fatty acid (FA) off the glycerol backbone of a triglyceride, diglyceride and monoglyceride, respectively.

The first association between Wnt and cancer was made, when Wnt-1 was described as an oncogene in murine breast cancer by Nusse and Varmus, 1982. Wnt furthermore acts upstream of Planar Cell Polarity (PCP) components (Humphries and Mlodzik 2018). These components arrange in a directional manner in cells, ultimately contributing to the polarity of the respective cells. Among its function in other tissues, Wnt is now understood to be strongly involved in lung development and, more importantly, maintenance (Raslan and Yoon 2020). Naturally, deregulation of Wnt in lung cancer has been shown to not only be involved in establishment of tumors, but also in angiogenesis, chemotherapy resistant cancer stem cells and therapeutic resistance in general (Rapp et al. 2017). There has been a great deal of interest in the Wnt pathway as a therapeutic target in cancers in general recently, owing to the importance and impact this pathway can have (Anastas and Moon 2013).

It has been previously shown that deregulation of a neutral lipase can influence the expression and activity of important kinases (Tomin et al. 2018). Given MGL's importance in signaling, particular focus was given to MGL during for this thesis. Additionally, it has been suggested that MGL was necessary for cancer cells to be able to maintain growth and migrate (Nomura et al. 2010). However, later findings suggest MGL to negatively influence PI3K/AKT signaling and thus cancer growth (Sun et al. 2013). The same research group later generated MGL knockout mice and showed that MGL deficiency resulted in a higher incidence of multiple different tumors, including that of the lung (R. Liu et al. 2018). The same paper also associated an activation of ERK and EGFR with the lack of MGL.

Based on the previous findings regarding MGL in lung cancer mentioned above and the knowledge that cancers can exhibit altered metabolic processes involving lipids, we hypothesized, that inhibiting MGL could reveal involvement of MGL in oncogenic signaling pathways, influencing growth and migration of lung cancer cells. To investigate potential effects of the loss of MGL function, we resorted to inhibition of MGL via the chemical JZL184, a selective inhibitor of MGL, in a panel of lung cancer cells. Cell growth and migration were examined with a cell viability assay and imaging approaches, while an LC-MS/MS method was utilized to uncover changes in cellular signaling in those cell lines that exhibited an altered phenotype *in vitro*.

Material and Method

Solutions

Lysis Buffer for Western Blot (WB):	8.775 mg/mL NaCl 1% Triton-X 0.1% SDS 50 mM Tris-HCl pH 8 1:100 Protease Inhibitor Cocktail (Sigma Aldrich) 1:200 Phosphatase Inhibitor Cocktail (Sigma Aldrich)
Transfer Buffer (1 L):	5.82 g/L Tris-base 2.93 g/L Glycine 0.375 g/L SDS 200 mL Methanol fill to 1 L with Aqua dest.
10x TBS (1 L):	24.2 g/L Tris-base 78.8 g/L NaCl pH 7.6 (with HCl) fill to 1 L with Aqua dest.
1x TBS-T (1 L):	100 mL TBS 1 mL Tween 20 fill to 1 L with Aqua dest.
Lysis Buffer for Phosphoproteomics (PP):	6 M GuHCl 10 mM TCEP 40 mM CAA 100 mM Tris-HCl pH 8.5
SDC Lysis Buffer for PP:	4% Sodium deoxycholate (w/v) 100 mM Tris-HCl pH 8.5
Isopropanol (ISO)	
EP-Enrichment Buffer:	48% TFA 8 mM KH_2PO_4

EP-Beads Buffer:	80% Acetonitrile (ACN) 6% TFA
EP-Wash Buffer:	60% ISO 5% TFA
EP-Transfer Buffer:	60% ISO 0.1% TFA
EP-Elution Buffer:	32.9% ACN 5% NH_4OH
SDB-RPS Load&Wash:	1% TFA in ISO
SDB-RPS Wash:	0.2% TFA 5% ACN
SDB-RPS Elution Buffer:	59.7% ACN 0.1244% NH_4OH
MS Loading Buffer:	2% ACN 0.3% TFA

Cell Culture

6 different lung adenocarcinoma cell lines were used, 4 primary adenocarcinoma cell lines – A549, A427, H441 and HCC827 – and 2 metastatic adenocarcinoma cell lines – H358 and H1299. A549 cells were purchased from CLS (Germany) and the other five were a kind gift from Dr. Hrzenjak and Dr. Leithner (Division of Pulmology, Medical University of Graz). Cells were cultivated at 37° C, 18% O_2, 5% CO_2 in 98% relative humidity for all experiments.

Cell lines were grown in RPMI-1640 medium (Sigma Aldrich), supplemented with 10% FBS and 1% L-Glutamine, with the exception of HCC827 cells, which were grown in DMEM (Gibco), supplemented with 10% FBS and 1% L-Glutamine.

MGL inhibition was established using 1 µM of the selective MGL inhibitor JZL184 (Selleckchem), dissolved in DMSO at 1 mM stock. For control cells the same volume of pure DMSO was added instead.

Cell Harvesting

Cells were washed 3 times with cold PBS, removing all residual PBS, then Lysis Buffer (WB) was added, the amount depending on the plate used (e.g. 200 µl for a 10 cm dish, or 80 µl per

well of a 12-well plate). Plates were left 20 minutes on ice before using a cell scraper to detach the cells from the plates and transferring the lysate to fresh Eppendorf tubes. Each sample was then sonicated for 10 seconds at 70% amplitude and centrifuged at 14,000 g for 5 minutes to pellet the cell debris. A 1:20 dilution of the lysate was taken for protein estimation, after which 1 µg/µl protein solutions were prepared for each sample, adding 1x Laemmli Buffer (4x Stock) and 1x Reducing Agent (10x Stock).

Cell Counting

Cells were counted with a CASY cell counter using 50 µl cell suspension in 1 ml CASYton solution.

Protein Estimation

All protein estimations were performed with a Pierce™ BCA Protein Assay Kit (Thermo Scientific) in a 96-well plate format according to manufacturer's instructions.

Lipid Droplet (LD) Staining

For LD staining $3*10^5$ cells were seeded on KOH-treated cover slips in 6-well plates 24 hours prior to imaging. Cells were then incubated with a 1:1000 dilution of BODIPY™ 493/503 (Thermo Scientific) for 10 minutes at 37° C and fixed for 10 minutes with 3.7% formaldehyde in PBS, followed by two washing steps with PBS. For mounting VECTASHIELD® antifade mounting medium containing DAPI (Szabo-Scandic) was used. Images were acquired using a Nikon A1+ confocal laser scanning microscope with a 405 nm diode laser and 450/50 BP filter for DAPI, a 488 nm argon laser with a 525/50 BP filter for BODIPY™ and a 60x CFI Plan Apochromat Lambda oil immersion objective. The settings for the z-stacks were chosen to fit the Nyquist criterion. The analysis was performed with the FIJI software (1.51h). For each image, a maximum intensity projection of the BODIPY™ channel was generated and a threshold was set using the Kapur-Sahoo-Wong (Maximum Entropy) method. The calculated values were used on the whole stack for lipid droplet volume quantification. Based on a nucleus count a quotient of lipid droplet volume per cell for each image was calculated.

Protein Gel Electrophoresis

Proteins were loaded on NuPAGE™ 4-12% Bis-Tris Gels (novex life technologies) and run with 1x NuPAGE™ MOPS SDS Running Buffer (novex life technologies).

Western Blot

Primary Antibodies (rabbit-antibodies) used were purchased from Cell Signaling Technologies (CST) and included ATGL (1:1,000), Phospho-SRC (Tyr416) (1:1,000), Phospho-AKT (S473) (1:1,000) and Phospho-EGFR (Tyr1068) (1:1,000). MGL-antibody (1:1,000) was purchased from Invitrogen, Phospho-ERK (Tyr204) (1:1,000) was purchased from Abcam and β-actin

antibody (1:5,000; mouse-antibody) was purchased from Sigma Aldrich. Anti-rabbit and anti-mouse antibodies coupled to horse radish peroxidase (HRP) (CST) were used as secondary antibodies in 1:3,000 dilution. Antibodies were diluted in TBS-T.

Amersham™ Protran™ 0.2 µm Nitrocellulose (GE Healthcare Life Science) membranes were blotted with Trans-Blot® SD Semi-Dry Transfer Cell (BioRad) for 1 hour 15 minutes at a constant 180 mA (220 mA for 2 membranes simultaneously) with a maximum of 25 V after soaking the membranes, filters and gel in transfer buffer.

Membranes were blocked with 5 % skim milk in TBS-T for non-phosphoproteins and 5% BSA in TBS-T for phosphoproteins for either 1 hour at room temperature (RT) or overnight at 4° C. Incubation with primary antibody was performed for 1 hour at RT or overnight at 4° C. Membranes were then washed for 5 minutes 5 times with TBS-T and subsequently incubated with secondary antibody for either 1 hour at RT or overnight at 4° C. Before detection, membranes were washed another 3 times for 5 minutes each. The two solutions contained in SuperSignal™ West Pico PLUS Chemiluminescent Substrate (Thermo Scientific) were mixed 1:1 and incubated for 5 minutes and then added to the membranes, which were scanned on a ChemiDoc Touch (BioRad). Membranes were stripped using Restore™ Western Blot Stripping Buffer (Thermo Scientific) for detection of non-phosphoproteins of the corresponding phosphoproteins for 7 minutes at RT and afterwards washed for 10 minutes 3 times.

The ImageLab software (BioRad) was used to quantify protein band intensities from the scanned images of the blots.

Scratch Migration Assay

Cells were seeded in 12-well plates at ~$4*10^5$ per well. After cells reached confluency a scratch was introduced down the middle of each well using a 100 µl pipette tip. Scratched off cells were discarded by aspirating the old medium and washing the plates once with PBS before adding fresh medium. Plates were then immediately imaged with an inverted light microscope, the imaged spots were marked and imaged again regularly for up to 72 hours. With the software FIJI (1.15h) the area not occupied by cells was then calculated and the percentage by which the gap had been closed was determined.

Cell Growth Evaluation

Cell proliferation was measured using the Cell Proliferation Kit I (MTT) (Roche). The kit was used as suggested in the kit's manual, although with $2*10^3$ cells (instead of the suggested $3*10^3$) seeded per well in 96-well plates and the absorbance measured at a wavelength of 550 nm.

Additionally, to establish growth curves, $8*10^4$ cells were seeded per well in 12-well plates and imaged continuously in the Cell Observer (Zeiss) for multiple days, utilizing custom scripts written by Jürgen Gindlhuber to determine the cell count.

Phosphoproteomics – Sample Preparation

H358 and A441 cells were seeded in 15 cm dishes and grown to ~80% confluency. Cells were then serum-starved for 30 minutes after which 1 µM JZL184 in 20 µL DMSO was added to 20 mL medium for 20 minutes. The same volume of only DMSO was added to the control cells. For harvesting, the dishes were put on ice and washed twice with cold PBS. 3,500 µL of Lysis Buffer (PP) were added, cells were detached using a cell scraper and collected in 5 mL tubes. Cells were then heated to 95° C for 5 minutes and afterwards put on ice. After sonicating each sample with 1.5 kJ at 90% amplitude (on ice) they were heated to 95° C for another 10 minutes.

For acetone precipitation, samples were initially centrifuged for 30 minutes at 3,500 g and 4° C and supernatants were transferred to clean tubes. Half of the supernatant´s volume of H_2O was added to dilute the samples. With 4 volumes of -20° C acetone proteins were precipitated overnight at -20° C. Precipitates were centrifuges at 7,000 g for 15 minutes at 4° C, discarding the supernatant. The resulting pellets were washed twice with -20° C 80% acetone and subsequently air dried at RT. Pellets were resuspended in SDC Lysis Buffer to reach a minimum protein concentration of 3.6 mg/ml and sonicated 3 times for 30 seconds at 80% amplitude.

Protein concentration was determined with Pierce BCA Protein Assay Kit (Thermo Scientific). 1 mg of protein per sample (enough for 2 LC-MS/MS measurements) were diluted to 280 µl with SDC Lysis Buffer and Trypsin was added in a 1:50 ratio (20 µg). Samples were left to digest overnight at 37° C at 1,500 rpm. 3 µl of digested samples were frozen for potential future proteome analysis (need to be desalted using SDB-RPS!).

For Phospho-Enrichment, the EasyPhos platform by Humphrey, Azimifar, and Mann (2015) was adapted. The digested samples were mixed with 400 µl ISO by vortexing for 30 seconds. 100 µl EP-Enrichment Buffer were added and vortexed again for 30 seconds, after which samples were centrifuged at 16,000 g for 15 minutes at RT, supernatants were transferred to clean tubes. 12 mg TiO_2-Beads per 1 mg protein were suspended in EP-Beads Buffer for a concentration of 0.5 mg/µl by sonicating for 1 minute in an ultrasonic bath. 24 µl of bead suspension were added to each sample, making sure to keep the beads in solution by pipetting and vortexing. After 5 minutes incubation at 40° C at 1,500 rpm samples were centrifuged at 2,000 g for 1 minute at RT and the supernatant was discarded. The beads were then washed five times by resuspending in EP-Wash Buffer, incubating for 30 seconds at RT at 1,400 rpm, centrifuging at 2,000 g for 1 minute at RT and carefully discarding the supernatant. After washing, 75 µl EP-Transfer Buffer were added to the beads, resuspending and then transferring them to a C8-Stage tip (self-packed, one layer of C8-material in 200 µl pipette tip with self-made adapter to fit on 2 ml tube). Using another 75 µl EP-Transfer Buffer the remaining beads were transferred to the same tip. Tips were then centrifuged at 1,500 g for 20 minutes (or until no liquid remained) at RT, discarding the flow-through. Tubes were replaced by fresh ones and phospho-peptides were eluted by adding 30 µl EP-Elution Buffer and centrifuging at 1,500 g

for 4 minutes (or until no liquid remained). The elution step was repeated a second time, after which samples were immediately dried in a speed vac until a maximum of 15 µl liquid remained (but not dried completely).

Immediately after phospho-enrichment samples were desalted by first being diluted with 100 µl SDB-RPS Load&Wash and then transferred to a SDB-RPS Stage Tip (self-packed, two layers of SDB-RPS material in 200 µl piptette tip with self-made adapter to fit on 2 ml tube). After centrifuging samples at 1,500 g until no liquid remained at RT, tips were washed with 100 µl SDB-RPS Load&Wash and repeating the centrifugation step. The washing step was repeated one more time with 100 µl of SDB-RPS Wash. Phospho-peptides were then eluted with 60 µl SDB-RPS-Elution Buffer into a fresh 2 ml tube with a glass vial insert. The samples were dried down for around 30 minutes in a speed vac.

Dry samples were either stored at -20° C until measurement or immediately resuspended in 10 µl MS Loading Buffer (for two injections of 4 µl), shaken for 2 minutes at 1,500 rpm and spun down, after which the glass insert was put into a LC injection vial and samples were measured.

Phosphoproteomics – Machine and Method

Chromatography was performed on an Ultimate 3000 RSLCnano system (Thermo Fisher Scientific) equipped with an Aurora Series UHPLC C18 column (250 mm x 75 µm, 1.6 µm, IonOpticks). Total LC-MS/MS measurement time was 133 minutes. Separation was carried out at 50 °C at a flow rate of 300 nl/min using the following gradient, where solvent A is 0.1 % formic acid in water and solvent B is acetonitrile containing 0.1 % formic acid: 0-18 min: 2% B; 18-100 min: 2-25% B; 100-107 min: 25-35% B, 107-108 min: 35-95% B; 108-118 min: 95% B, 118-118 min: 95-2% B; 118-133 min: 2% B. Mass spectrometry was performed on a Maxis II qTOF instrument (Bruker) set to fragment the top 20 most abundant peptides of each full spectrum within one cycle. Database search was done with MaxQuant 1.6.1.0 (Cox and Mann 2008), searching the public Swissprot database with taxonomy *Homo sapiens* and common contaminants (downloaded on 16.04.2019, 20482 sequences). Carbamidomethylation on Cys residues was set as fixed modification, oxidation on Met residues and phosphorylation on Ser/Thr residues as variable modification. Detailed decoy database search criteria included: trypsin; max missed cleavage sites: 2; acceptance parameters for identification: 1% PSM FDR; 1% protein FDR.

Phosphoproteomics – Data Analysis and Visualization

To statistically analyze the phosphoproteomics data obtained after MaxQuant search of the LC-MS/MS data, the phospho(ST).txt file was imported into the Perseus software (1.6.5.0) (Tyanova et al. 2016). The phospho(ST) table was filtered for contaminant and reverse peptides found by the decoy database search. Intensities were $\log_2$ transformed to lower effect of outlier values and filtered for a localization probability of > 75% and for 3 valid values in at least one

group. Missing values were imputed from the downshifted normal distribution of the data (width 0.6, downshift 1.8) and values were normalized by subtracting the median. Significantly changed phosphopeptides by MGL inhibition were obtained by two-sided Student´s t-test (S0 0.1) and permutation-based FDR (5%).

Hierarchical cluster analysis was performed by matching the matrix containing the significantly changed phosphopeptides to the matrix obtained after imputing the missing values in the original data. Every value in the resulting matrix was z-scored (normalized by subtracting the mean, then dividing by the standard deviation), after which Euclidian distance hierarchical clustering was used to generate a heatmap. A matrix containing the peptides in the heatmap was generated and matched to the matrix obtained after imputing the missing values in the original data. A Fisher exact test (Benjamini-Hochberg correction, FDR 2%) was performed to find significantly enriched GO, KEGG and Reactome terms. This list of phosphopeptides was sorted by p-value to generate **Supplemental Table 1** and **Supplemental Table 2**.

The matrix generated after imputation of missing values was exported and loaded into a separate Perseus entity alongside the 9606.protein.links.v11.0.txt.gz file from the String database (Szklarczyk et al. 2019) (downloaded on 16.07.2019) to calculate "signaling scores" based on 10,000 permutations using the PHOTON software plug-in for Perseus (Rudolph et al. 2016). Resulting protein-interaction networks were visualized with Cytoscape software (Shannon et al. 2003).

For additional examination of protein interactions, the KSEA app (Wiredja, Koyutürk, and Chance 2017; Hornbeck et al. 2015) was implemented as an automated R script to allow offline analysis of the phosphoproteomics data. First, the log_2 transformed matrix was exported and loaded into a separate Perseus entity where the values were normalized by subtracting the mean of every column from the values. The data was then filtered for 3 valid values in at least one group, after which missing values were imputed from the downshifted normal distribution of the data (width 0.6, downshift 1.8). Because KSEA requires p-values for each peptide, a two-sided Student's t-test (S0 0.1) with permutation-based FDR (5%) was performed. The mean of each group was then calculated and the difference between the mean of the treatment group and the mean of the control group was calculated. The columns "Gene name", "Protein" and "Positions within proteins" were expanded to not contain multiple entries. Log_2 transformation of the data was reversed in the last step (by raising 2 to the power of the respective value), as KSEA does not work with log transformed data. The resulting matrices for H358 and H441 respectively were exported and used as input for the KSEA R script.

Results

Comparing Lung Cancer Cell Lines: Lipolysis and Signaling Proteins

Lipid droplet content and lipolytic profile differ between different lung cancer cell lines

To distinguish which cancer cell line would be more likely to be dependent on lipid accumulation and/or lipid hydrolysis, our first goal was to compare the lipid droplet (LD) content of a lung cancer cell panel and the expression of the key lipolytic enzymes adipose triglyceride lipase (ATGL) and monoacylglycerol lipase (MGL) in these cells.

Western Blot analysis showed that all cell lines expressed ATGL, albeit at greatly varying levels. For clarity, data was normalized to the expression levels in A549 cells. (**Figure 1**). Interestingly, unlike ATGL, which was expressed in all cell lines, MGL was virtually gone in A427 and H1299 cells, while HCC827, H358 and H441 did express MGL, although significantly less than A549 cells. This suggests that MGL could potentially have a more cancer etiology- or cell line-dependent role in cancer metabolism.

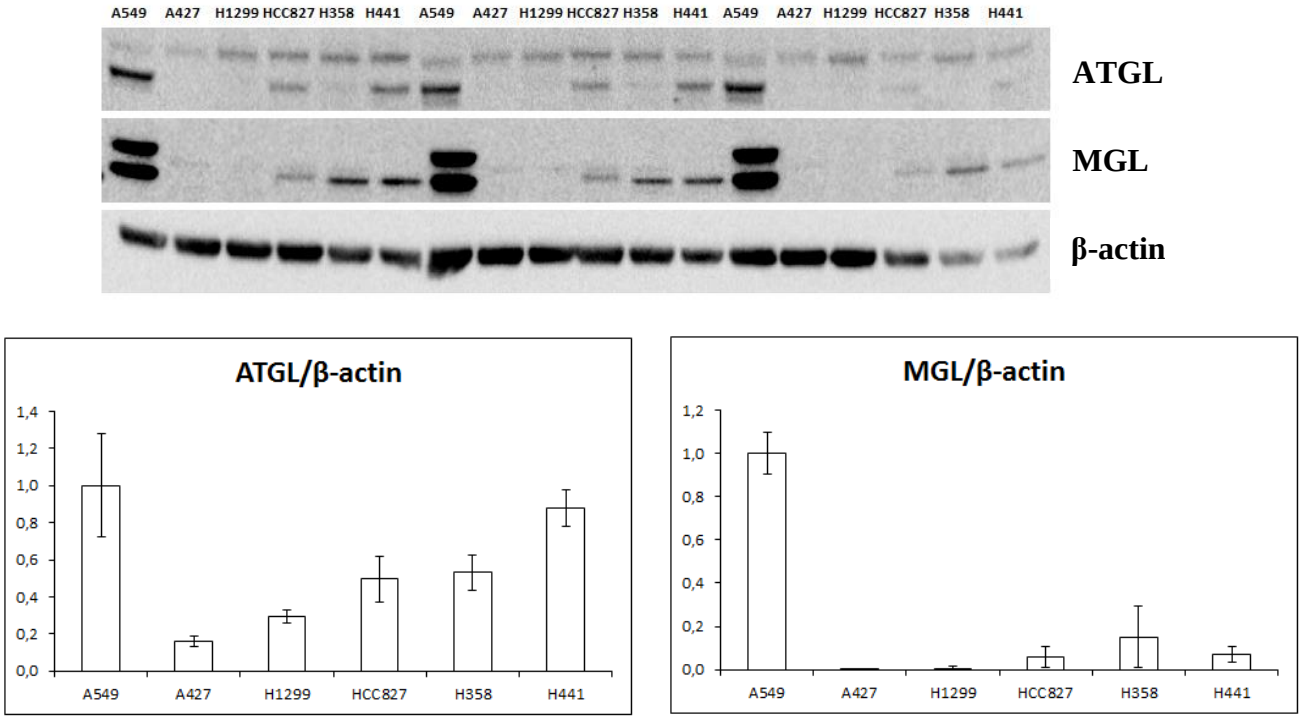

Figure 1: ATGL and MGL expression vary in lung cancer cell lines. Cells were grown to ~80% confluency, harvested and 20 µg of protein were loaded on the gel. Ratios of ATGL to β-actin and MGL to β-actin were taken per sample, means and SD were calculated and all ratios were normalized against A549 ratio for clarity. Mean ± SD; n=3

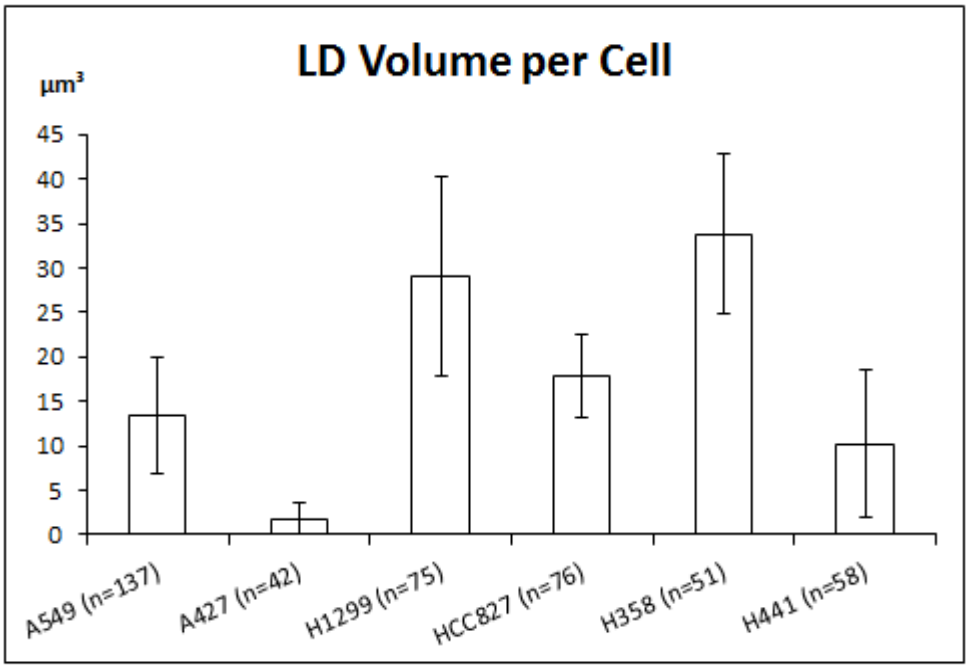

Figure 2: Lipid Droplet content is hugely different between lung cancer cell lines. $3*10^5$ cells were seeded on cover slips, grown for 24 hours, stained with BODIPY™ and imaged on a NIKON A1+. From microscopy images, volume of LDs was calculated and normalised on the number of nuclei counted. Mean ± SD; n shown individually per cell line

Additionally, the LD content of the cells was determined using BODIPY™ dye on a NIKON A1+ Microscope to image the cells. The number of nuclei and volume of LDs was determined from the microscopy images with help of Jürgen Gindlhuber. The tested cell lines ranged in LD content from only a few µm³ per cell to over 30 µm³ per cell (**Figure 2**). A427 cells, which appear to be least dependent on lipolysis among the tested cells (**Figure 1**), contain the least amount of storage lipids, at 2 µm³ per cell. Furthermore, although A549 cells showed the highest expression level for both ATGL and MGL, proteins associated with LDs, they are only in the center span for LD content with 13 µm³ per cell. H441 and HCC827 are also in within the center of the range with 10 µm³ and 18 µm³ LD per cell, respectively. H1299 cells contain 29 µm³ LDs per cell on average, H358 cells average at 34 µm³ per cell, both with quite large standard deviations. The varying numbers and sizes of LDs in the different cell lines was already apparent when looking at the microscopy images, a sample of which is provided in **Figure 3.**

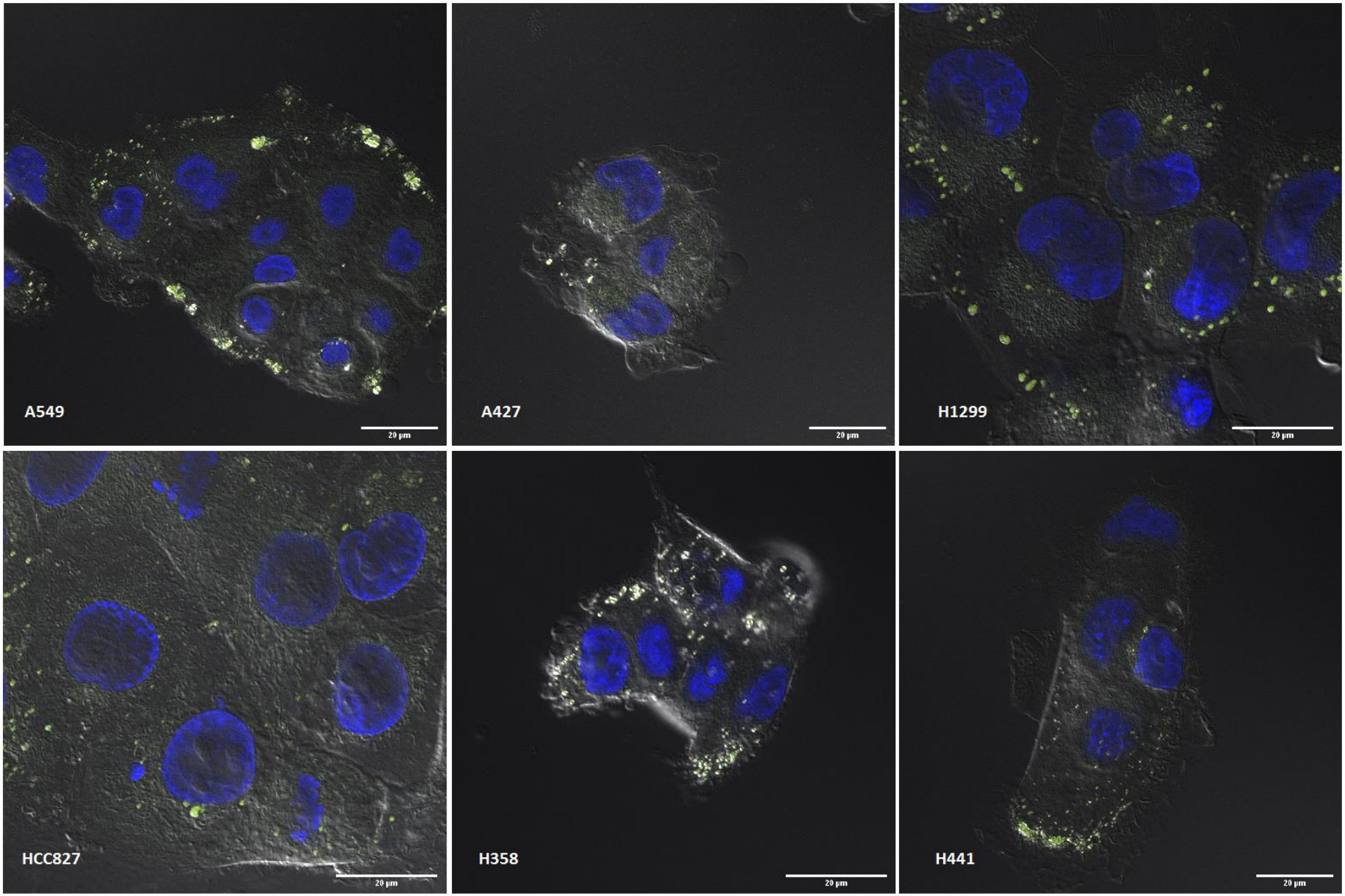

Figure 3: Lipid droplet content is visually different between lung cancer cell lines. Lipid droplets were stained using BODIPY™, after which cells were fixed with 3.7% formaldehyde and nuclei were stained with DAPI. Images were acquired on a Nikon A1+ confocal laser scanning microscope and edited using the FIJI software.

Expression Levels of Signaling Proteins Vary in Different Lung Cancer Cell Lines

In addition to the lipase and LD profiles, we examined the activation status of several signaling kinases SRC, AKT, ERK and EGFR , the majority of which has already been reported to be implicated in cross talk between deregulated lipolysis and pro-oncogenic signaling (Tomin et al. 2018; Sun et al. 2013; Du et al. 2015; Menendez 2010). Furthermore, we also addressed the expression of the most prominent tumor suppressor p53, which has also been brought in correlation with deregulated lipolysis in cancer (Di Leo et al. 2019). The ratio of the protein of interest or the phosphorylated form to β-actin was calculated from the protein bands' intensities (**Figure 4**).

Tyrosine kinase SRC is phosphorylated at the activating site Tyr416 to varying extent and with large variance across the cell line panel. Wild-type A549 cells appear to be almost entirely devoid of SRC phosphorylation at this residue. Phosphorylation of Proteinkinase B – AKT – was fluctuating somewhat greatly between cell lines. A549, A427, HCC827 and H441 cells show comparable levels of AKT phosphorylation at Ser437. The metastatic cell lines H1299 and H358 seem to have AKT more strongly activated (by two to four times) than the other cell lines, however with large variance and thus low confidence.

Furthermore, the active forms of the membrane-bound growth factor receptor EGFR and the kinase ERK (MAPK) as well as general expression of the tumor suppressor p53 were examined. The presence of the activating phosphorylation at Tyr1068 was found in all cell lines at different levels, with H358 and H441 cells showing the highest levels of pEGFR among the tested cell lines. When Phospho-ERK (Tyr204) was examined, A427 and HCC827 showed the lowest pERK to β-actin ratio, while the levels of other cell lines were comparable to each other. However, all ratios calculated are within margins of error of one another. p53 expression was also examined with this immunoblotting analysis, revealing comparable levels in A549 and A427 cells. While HCC827 and H441 cells have a high variability between samples, their mean p53-to-β-actin ratios are considerably higher than those in the other cell lines. On the other hand, no p53 was detectable in H1299 and H358 cells, which is expected as they are reported to be p53-null (Mitsudomi et al. 1992; Bodner et al. 1992)

In a nutshell, the overall activation profile of kinases in the lung cancer cell panel differs between individual cell lines. Among the lipases, MGL expression seems to differ more greatly within the cell lines tested compared to ATGL, with A549, H441 and H358 expressing the highest MGL levels observed in the panel. With previous publications suggesting cross talk between MGL and pro-oncogenic signaling and the results shown below indicating that those three cell lines are most sensitive to changes in MGL activity, we opted to investigate how signaling in these three cell lines would be affected if MGL activity was inhibited.

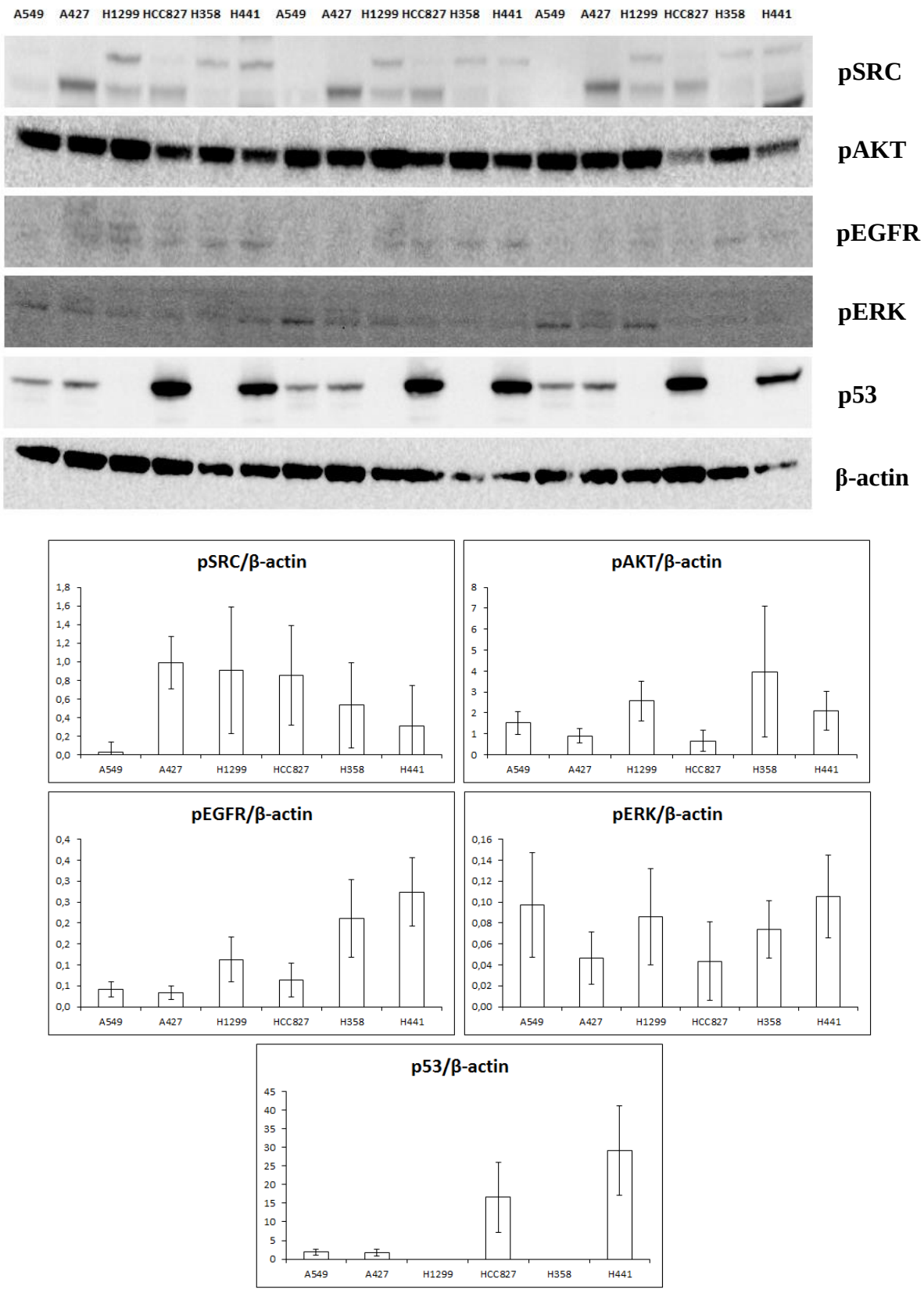

Figure 4: Expressions of pSRC (Tyr416), pAKT (Ser437), pEGFR (Tyr1068), pERK (Tyr204) and p53 differ within lung cancer cells. Cells were grown to ~80% confluency, harvested and 20 µg protein were loaded on the gel. Ratios of proteins to β-actin (loading control) were taken per sample, means and SD were calculated. Mean ± SD; n=3

Cellular Effects of Inhibition of MGL Activity: Proliferation, Migration and Protein Levels

Lung Cancer Cell Growth is Marginally Influenced by MGL Activity

To elucidate, if and to what extend MGL activity impacts growth of lung cancer cells, all cell lines were treated with the MGL inhibitor JZL184 and proliferation was tested every 24 hours using an MTT cell proliferation kit over a period of up to 72 hours. The first test revealed greatly fluctuating growth rates for all cells lines. H358 and H441 cells however trended toward a faster growth upon MGL inhibition after 72 hours (**Figure 5**). For those two cell lines, in addition to A549, the MTT test was repeated for a total of n=9 replicates for those cell lines, where the

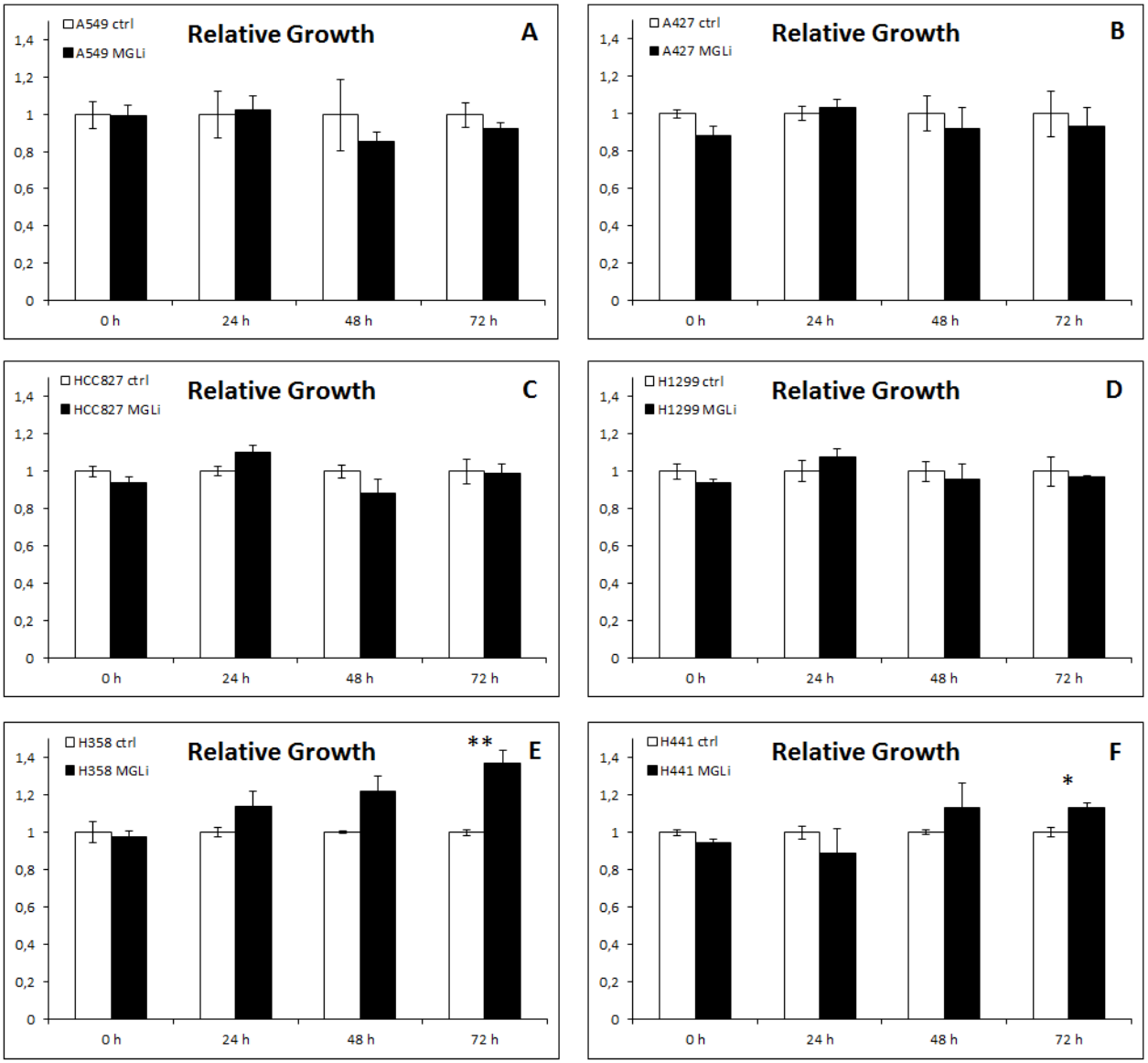

Figure 5: Growth of lung cancer cells with MGL inhibition (MGLi) and without (ctrl) determined with an MTT assay over 72 hours. For each timepoint, a separate 96-well plate was used. 2000 cells were seeded per well. Medium was changed every 24 hours where necessary to maintain MGL inhibition by counteracting inactivation of JZL184. Means of MGLi for each timepoint were normalized to the means of ctrl for the respective timepoint. A549 (A), A427 (B), HCC827 (C), H1299 (D), H358 (E), H441 (F). Mean ± SEM; n = 3; *: $p < 0.05$; **: $p < 0.01$

same trend could be replicated (**Figure 6**). While statistical significance was not reached for H441 cells, the growth advantage of H358 cells could be replicated with statistical significance.

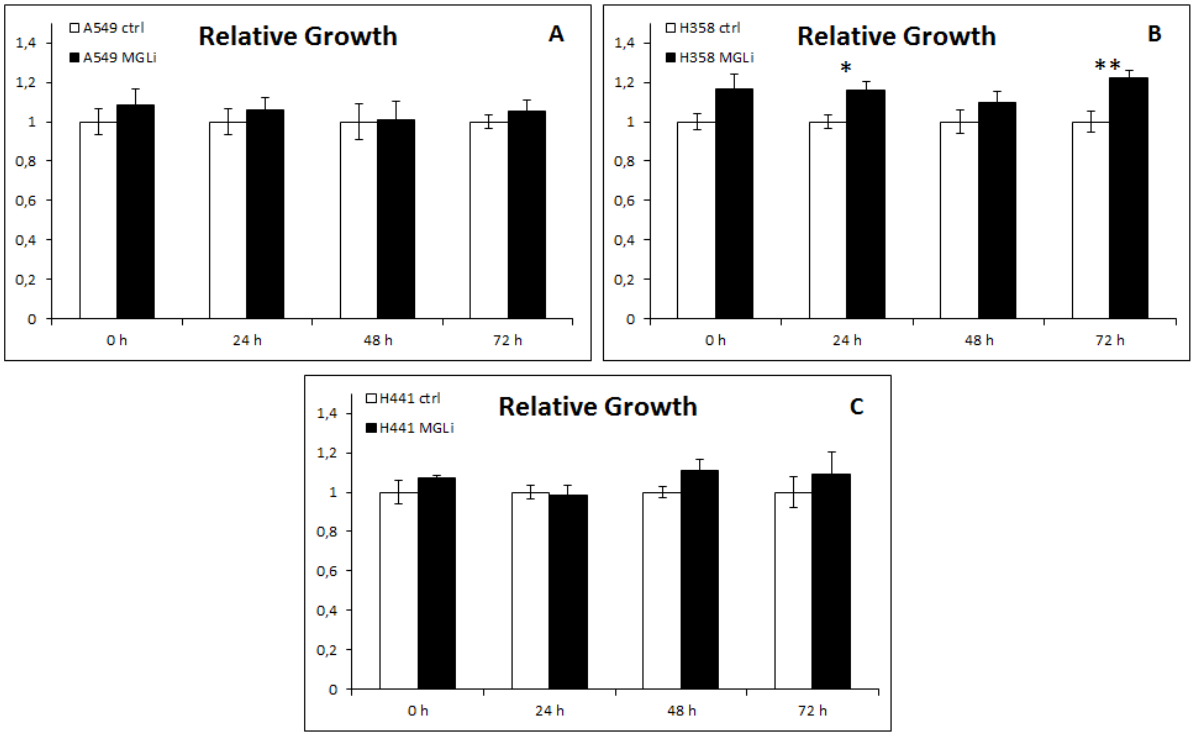

Figure 6: Slight growth advantage of H358 and H441 cells upon MGL inhibition (MGLi) over control (ctrl) cells was reproducible when performing an MTT assay with 6 replicates over 72 hours and combining data for total n=9. For each time point, a separate 96-well plate was used. 2000 cells were seeded per well. Medium was changed every 24 hours where necessary to maintain MGL inhibition by counteracting inactivation of JZL184. Means of MGLi for each timepoint were normalized to the means of ctrl for the respective timepoint. A549 (A), H358 (B), H441 (C). Mean ± SEM; n = 9; *: $p < 0.05$; **: $p < 0.01$

A549 cells seem to exhibit no significant increase in proliferation if MGL activity is inhibited compared to the uninhibited control cells over a period of 72 hours (**Figure 5**, **A**). A427, HCC827 and H1299 cells all varied in their growth over the 72 hours tested, with no significant differences between MGL-inhibited cells and control cells (**Figure 5**, **B - D)**. For H358 and H441 cells however a trend of increased proliferation started to show after 48 hours. This trend culminated in a significantly greater proliferation in those two cell lines when MGL activity was hampered (**Figure 5**, **E** & **F**). In H441 cells, the increase in proliferation was just over 13% compared to the control group, with H358 cells exhibiting a growth increase of almost 37%.

In a separate experiment, H358 and H441 cells were treated with JZL184 and imaged hourly for multiple days to generate a growth curve. The slope of each curve was calculated, and the mean of each condition was taken to compare between the control group and the treatment group (**Figure 7**). While inhibition of MGL resulted in H358 cells growing faster by about 7%, the same effect was more pronounced in H441 cells, with an increase of almost 17% in growth

rate. Taken together with the MTT results, this experiment supports the assumption, that growth in these lung cancer cells is linked to MGL activity.

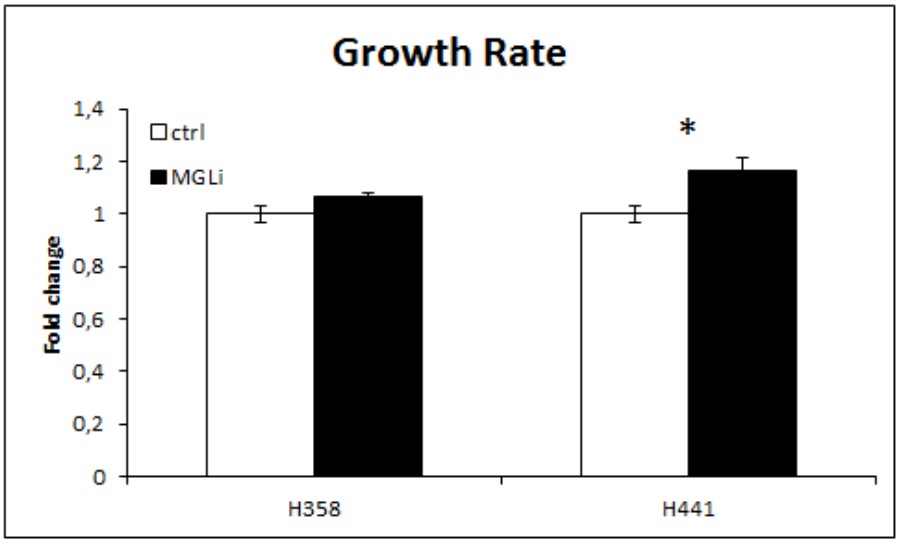

Figure 7: H358 cells grow marginally faster when MGL activity is inhibited, while H441 cells show a significant boost in growth after the same treatment. Cells were imaged in technical replicates in the Cell Observer over 24 hours. For both the control group (ctrl) and the treatment group (MGLi) the means of the maximal slopes of each resulting growth curve were taken and normalized against the respective control group. Medium was changed every 24 hours to counteract inactivation of JZL184 to maintain MGL inhibition. Mean ± SEM. n = 21 (3 replicates times 7 spots per well)

Migration Ability Is Independent of MGL Activity

In addition to the described growth experiments, the migratory abilities of A549 cells and of those cell lines that exhibited a growth advantage upon the inhibition of MGL, H358 and H441, were tested by growing them to 100% confluency and introducing a "wound" (scratch) using a pipette tip. Following that a series of microscopy images were taken and used to calculate the area of the "wound" over time with the help of a custom ImageJ program written by Jürgen Gindlhuber.

A549 lung cancer cells appeared to migrate faster when MGL activity was inhibited, but this trend was not observable at every timepoint (**Figure 8**). H358 cells remained generally within margins of error when putting the control and treatment group side by side, with later timepoints hinting toward faster migration with MGL inhibited as well. On the other hand, H441 cells that were treated with JZL184 did seem to migrate marginally slower compared to the control. None of these results showed any statistical significance, however. The reason for this may as well be a result of this experiment not measuring solely the migratory capabilities of the cells but a combination of migration and proliferation.

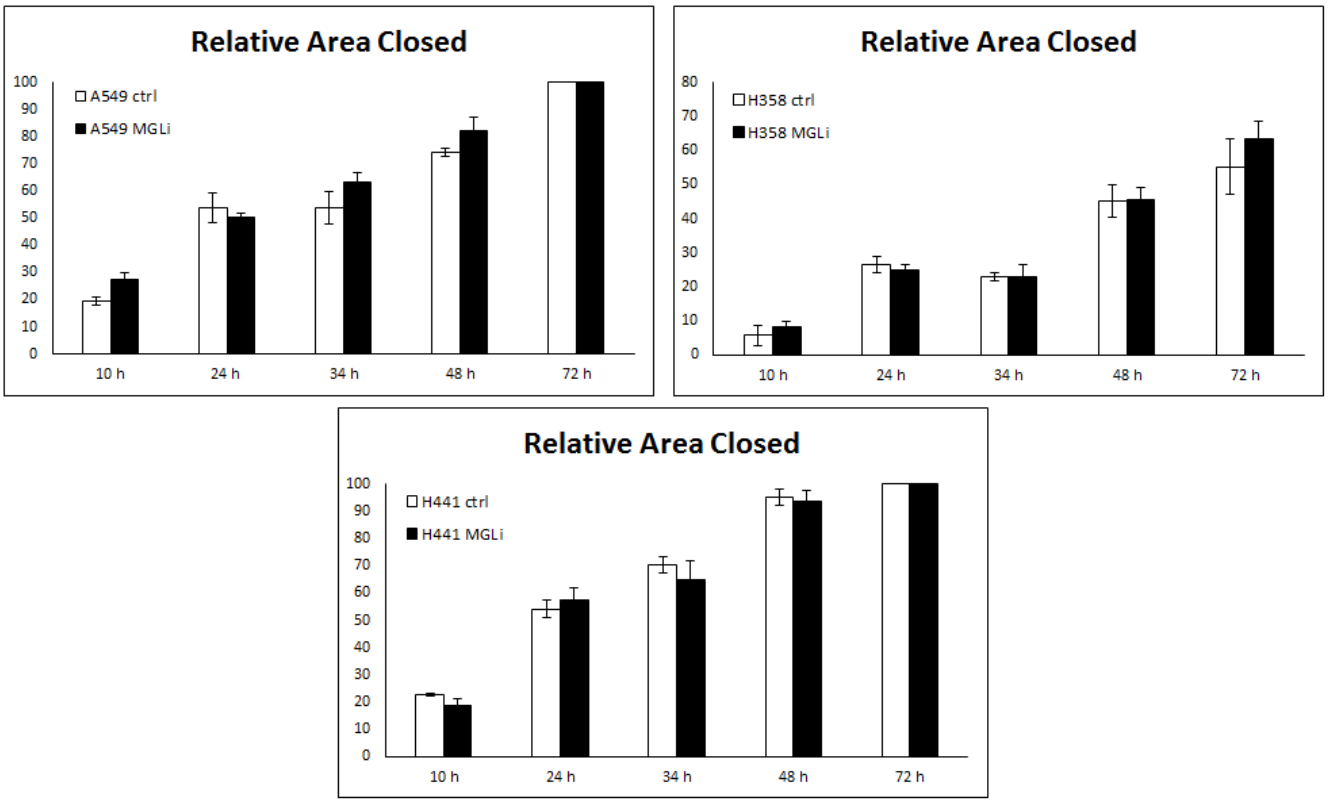

Figure 8: No effect of MGL inhibition on migratory abilities of lung cancer cells. After cells were grown to confluency, a scratch was introduced. Microscopic imaging was used to determine the area of the scratch for 72 hours total. Percentage of the area closed is blotted against respective timepoints. Mean ± SEM. n = 3

Immunoblotting Reveals No Effect on Kinase Activation

Based on the previous Immunoblotting experiments that were done to outline oncogenic protein expression and activation levels in different lung cancer cell lines, the same was addressed upon MGL inhibition. For this purpose, 1 µM MGL inhibitor JZL184 was administered to A549, H358 and H441 cells for 24 hours prior to harvesting for Western Blot (**Figure 9**).

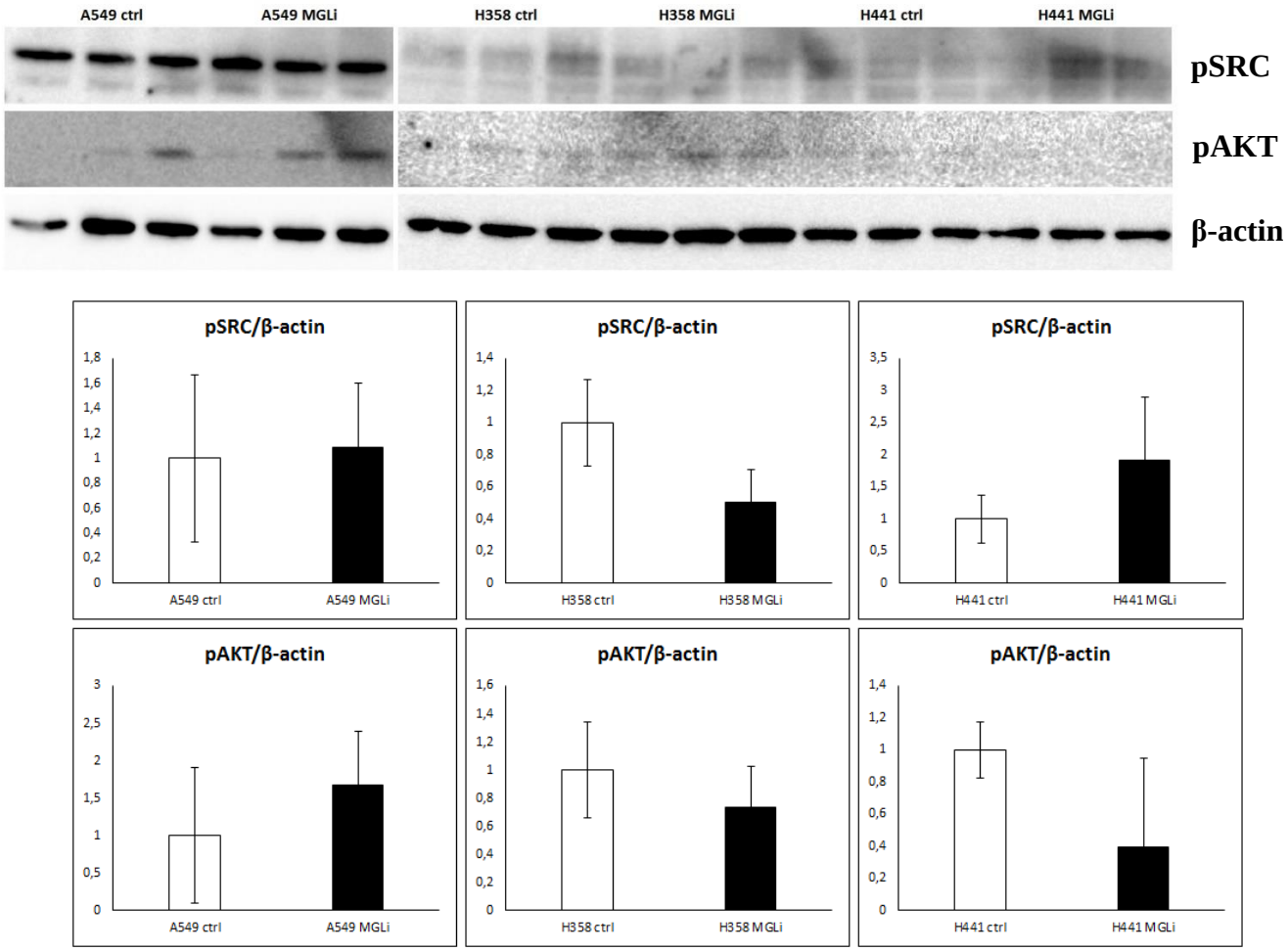

Figure 9: MGL inhibition in A549, H358 and H441 cells does not affect SRC and AKT activity. Cells were grown to ~80% confluency, incubated with 1 µM JZL184 for 24 hours, harvested and 20 µg of protein were loaded on the gel. Ratios of pSRC (Tyr416) and pAKT (Ser437) to β-actin (loading control) were taken per sample, means and SD were calculated and normalized to respective control group. Mean ± SD; n=3

In A549 cells, inhibition of MGL had no observable effect on pSRC expression compared to control cells. While pAKT expression trended toward being higher in A549 cells with inhibited MGL, the variance between replicates was too big for any sound conclusion. H358 cells showed a slight drop in both pSRC and pAKT expression. pSRC expression was lower by around 50% when MGL activity was hampered, without reaching statistical significance, however. The difference in pAKT expression in H358 between the treatment and control group was even

smaller than in pSRC expression, although with the same trend of AKT activation dropping upon MGL inhibition. Lastly, pSRC in H441 was increased almost 2-fold with MGL inhibition compared to the control. The considerably large variance prevents this from being statistically significant, as well. On the other hand, pAKT was as low as 40% from the pAKT in the control cells, however significance was not reached for this result either.

These Western Blot analyses were repeated multiple times (data not shown), with varying results. No conclusive statement could be made from the Western Blots considering pSRC and pAKT expression in those 3 cell lines.

Also, in consideration of the LC-MS/MS phosphoproteomics experiment performed later, the cells were again treated with JZL184, however only for a period of 20 minutes, the same duration used for the phosphoproteomics experiment. The cells were then again examined via Immunoblotting (data not shown). The resulting Western Blots did not show any significant differences in pSRC and pAKT expression in A549, H358 and H441 when MGL was inhibited.

In total, pSRC and/or pAKT expression do not seem to be responsible for the previously observed growth advantage of H358 and H441 cells with hampered MGL activity. Therefore, H358 and H441 cells were subjected to phosphoproteomics when MGL activity was inhibited to potentially establish a link to the differences in proliferation.

Phosphoproteome:
Potential Involvement of MGL in Wnt Signaling Pathway

Based on the fact, that H358 and H441 cells tended to react to MGL inhibition in regard to proliferation and migration, those two cell lines were chosen for a LC-MS/MS phosphoproteomics analysis to uncover changes in phosphorylation of proteins that could be linked to oncogenic signaling. Cells were grown close to 80% confluency, at which point fresh medium was added containing 1 µM JZL184 to inhibit MGL activity. To observe the short-term signaling effects of the treatment, cells were harvested 20 minutes after administering JZL184, rather than incubating for 24 hours, which would reflect a steady-state change. Within 24 hours, any changes in signaling pathways would most likely be counteracted by regulating pathways, which is another reason why the 20 minutes incubation period was chosen. Control cells were prepared identically to cells treated with JZL184, except for adding only DMSO (20 µL) in place of JZL184 (0.1% DMSO in medium).

After the LC-MS/MS run and the MaxQuant search were completed, the resulting "Phospho (ST)Sites.txt" was loaded into Perseus to analyze. For each sample, the total intensities per phosphopeptide were loaded instead of the intensities for multiplicities, i.e. not distinguishing how many phosphorylations were on one specific peptide.

To test, whether any differences between sample groups were due to biological changes induced by the inhibition of MGL activity or random effects resulting from inconsistency between replicates, a Principal Component Analysis was performed. For H358 cells, replicates of the control group (c) showed great consistency among themselves. Although the JZL184-treated replicates (MGLi) were quite separated from each other, a clear discrimination between control and treated samples could be made through the first component. (**Figure 10**, **A**). H441 cell MGLi samples grouped decently together, with c samples being more separated. Still, a clear separation between groups in the first component could be observed (**Figure 10**, **B**). By clustering of the respective groups for the two cell lines any differences between the treated and untreated groups are more likely be due to actual discrepancies in the biology of the cells tested rather than due to technical variability.

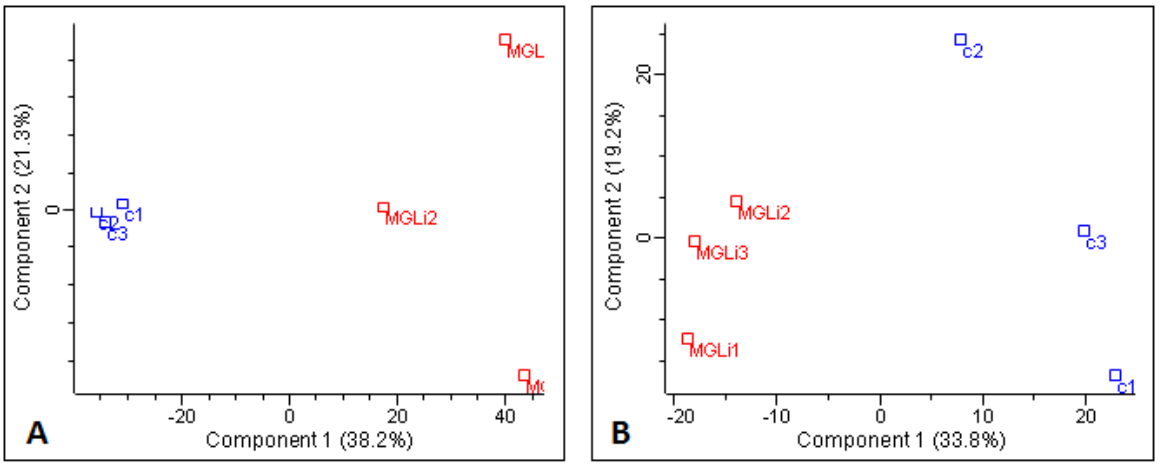

Figure 10: Replicates of Phosphoproteomics MS samples for H358 (A) and H441 (B) cells clustered in Principal Component Analysis (PCA). PCA of control cells (c1-c3) vs. treated cells (MGLi1-MGLi3) generated in Perseus.

Next, a two-sided Student's t-test (S0 0.1, permutation-based FDR 5%) was performed on peptide level. Before performing the t-test, the data was filtered for 3 valid values in at least one group for each cell line. Out of the resulting 1.965 and 609 peptides, 64 and 25 were found to be significantly changed between groups for H358 and H441, respectively. Heatmaps of differentially phosphorylated peptides are shown in **Figure 11** and **Figure 12**. Intensities were normalized by z-scoring on the rows of the data before creating the heatmap, which then represents how many standard deviations any row's value lies from that row's mean value. In H358 the phosphosite with the greatest difference in z-score between the treatment and control group was Ser756 of the Protein kinase C-binding protein 1 (ZMYND8). The fold change from control cells to treated cells for this peptide was calculated to be 12.47 after imputation of missing values. Looking at H441, Ser1218 of Rho GTPase-activating protein 5 (ARHGAP5) differs most between groups with a fold change of 20.17 between treatment and control. Among the phosphopeptides that were significantly different in their abundance after MGL inhibtion in H358 were for example peptides of the transcriptional regulators FOXK1 and FOXK2. While Ser101 of FOXK1 showed a fold change of 10.12 in the MGL-inhibited cells, the residue Ser428 of the FOXK2 peptide exhibited a fold change of 10.69 in treated cells vs. in the control cells. The same peptide of FOXK1 was found in H441 cells; in these cells the Ser101 was more phosphorylated, with a fold change of 17.52 in MGL-inhibited cells, however. Additionally, a peptide containing Ser412 of the scaffolding protein ARRB1, which is involved in SRC, ERK and AKT signaling was detected in H441, with a fold change of 17.83 in cells treated with JZL184. Of specific note is a phosphopeptide found in both cell lines, which is part of the Catenin delta-1 (CTNND1, henceforth δ-catenin) protein phosphorylated at Ser899. Nothing is known about this specific site yet, neither in humans nor in mice. δ-catenin protein takes part in regulating cell-cell adhesion and acts within the Wnt pathway. This result thus first hinted at a potential effect of MGL activity on Wnt signaling.

Performing a GO enrichment analysis of the cluster that contained phosphopeptides that were more abundant in cells with MGL inhibited revealed in both cell lines GO terms referencing Wnt signaling. Aside from that, adherens junction terms were enriched in both cell lines alike, as well as vascular endothelial growth factor receptor (VEGFR2) response (**Supplemental Table 1**, **Supplemental Table 2**).

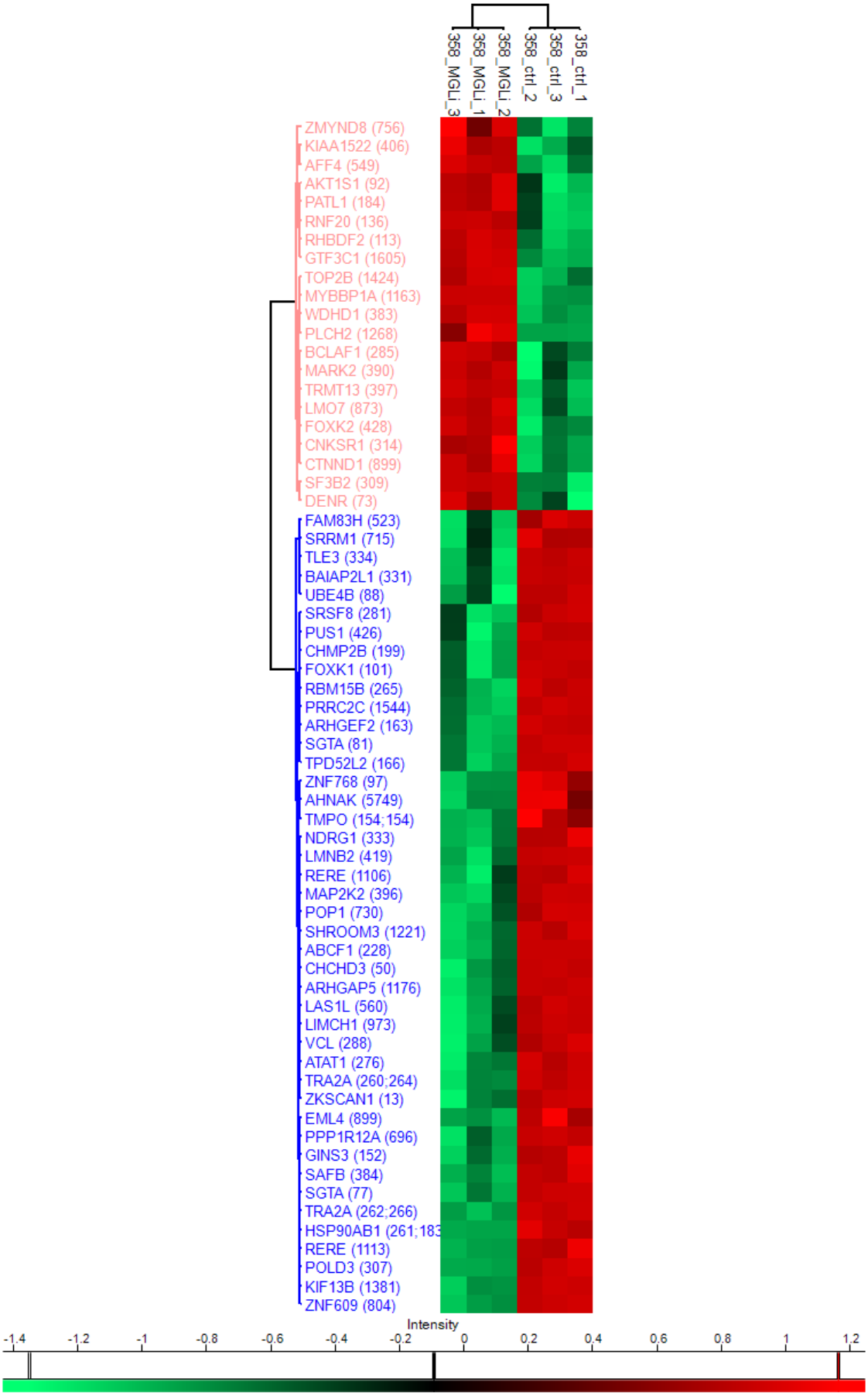

Figure 11: Inhibition of MGL activity leads to a number of peptides being more (red) or less (green) phosphorylated in H358. Significantly more or less phosphorylated peptides in MGL inhibited cells (MGLi) and in control cells (c). Intensities were z-scored, heatmap generated 2 clusters of peptides.

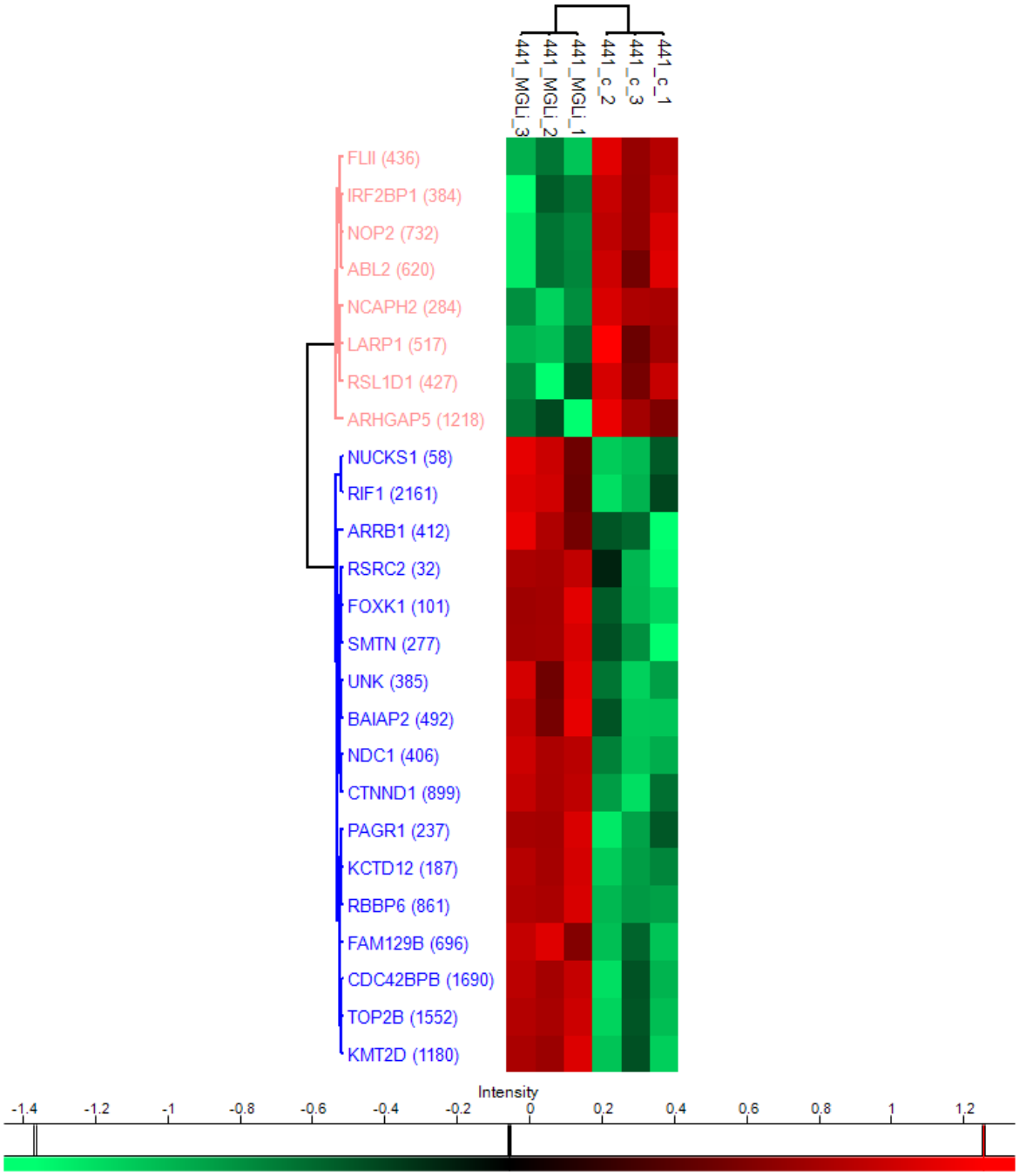

Figure 12: Inhibition of MGL activity leads to a number of peptides being more (red) or less (green) phosphorylated in H441. Significantly more or less phosphorylated peptides in MGL inhibited cells (MGLi) and in control cells (c). Intensities were z-scored, heatmap generated 2 clusters of peptides.

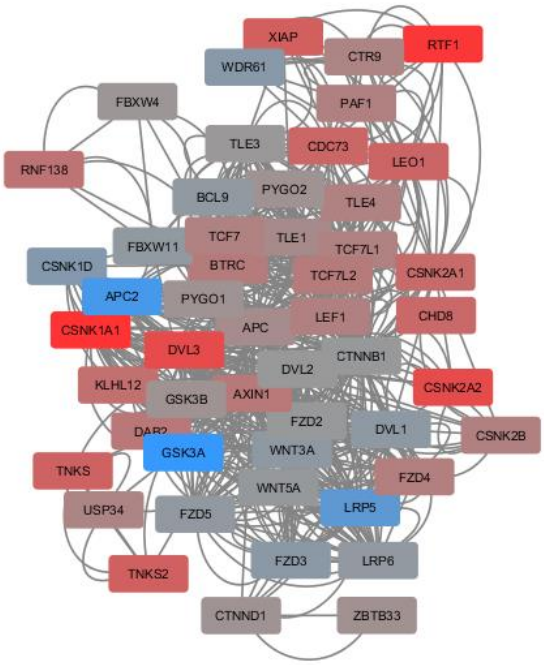

Figure 13: Several proteins annotated with the keyword "Wnt" were either more or less active in signaling when MGL was inhibited in H441 cells according to PHOTON scores. "Signaling scores" were calculated with 10,000 permutations in PHOTON within Perseus. The resulting network was loaded into Cytoscape, filtered for keyword "Wnt" and colored in accordance with the difference in mean "signaling score" between the group of JZL-treated cells (MGLi) and the control group (ctrl). Red indicates "signaling scores" higher in MGLi, blue indicates "signaling scores" higher in ctrl.

Utilization of the PHOTON add-in for Perseus mapped the experimental dataset to the entire protein interaction network of the human proteome. The resulting networks were loaded into Cytoscape and the difference in mean "signaling scores" between treatment and control group was used as basis for visualization. Since the network contains over 17.000 proteins linked by known interactions, proteins mapped with the keyword "Wnt" was put in a sub-network for both H358 and H441 cells, as this was the pathway that seemed to be enriched in both cell lines. In H441 cells, among "Wnt"-annotated proteins that had the most positive "signaling score" difference from treatment to control (red) – meaning they participate more in signaling in MGL-inhibited cells than in control cells – were casein kinase I isoform alpha (CSNK1A1/CK1α) and RNA polymerase-associated protein RTF1 homolog (RTF1) (**Figure 13**). RTF1 is a component of the PAF1 complex, which is required for transcription of Wnt target genes. As is known, CSNK1A1 phosphorylates β-catenin, a central player in the Wnt pathway (X. Liu et al. 2020). Proteins partaking less in signaling processes when MGL was inhibited are indicated with blue color in the same figure. The two most prominent proteins here are glycogen synthase kinase-3 alpha (GSK3A) and adenomatous polyposis coli protein 2 (APC). Both proteins regulate β-catenin levels in the cytosol by playing a part in inducing β-catenin degradation.

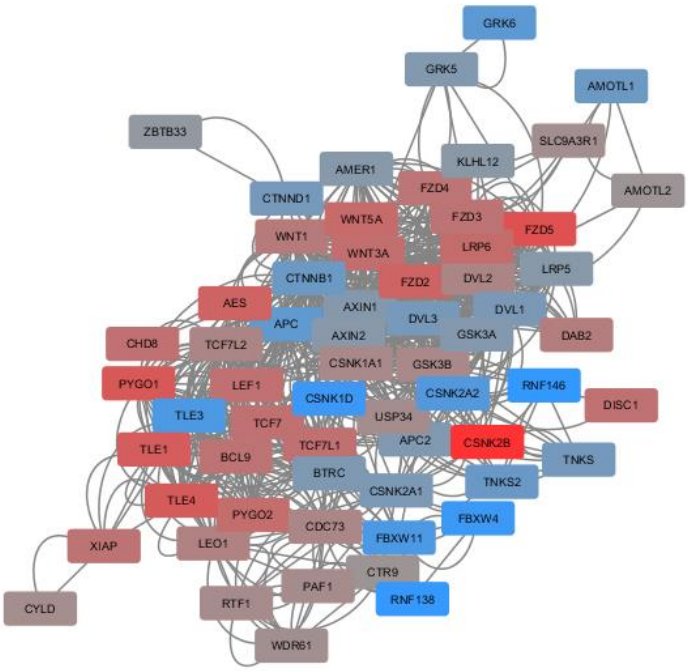

Figure 14: Several proteins annotated with the keyword "Wnt" were either more or less active in signaling when MGL was inhibited in H358 cells according to PHOTON scores. "Signaling scores" were calculated with 10,000 permutations in PHOTON within Perseus. The resulting network was loaded into Cytoscape, filtered for keyword "Wnt" and colored in accordance with the difference in mean "signaling score" between the group of JZL184-treated cells (MGLi) and the control group (ctrl). Red indicates "signaling scores" higher in MGLi, blue indicates "signaling scores" higher in ctrl.

The same analysis in H358 revealed one protein with an obviously higher activity in signaling after MGL activity inhibition (red), namely casein kinase II subunit beta (CSNK2B/CK2β) (**Figure 14**). Like CK1α, CK2β also phosphorylates β-catenin and thus affects Wnt signaling, however through different interactions with the pathway. Some other proteins that were less active in signaling after JZL184 was administered (blue) include other casein kinases (CSNK1D and CSNK2A2), E3 ubiquitin-protein ligases (RNF138 and RNF146) and F-box/WD repeat-containing proteins (FBXW4 and FBXW11) among others, that all directly or indirectly regulate Wnt signaling.

Lastly, the kinase-substrate enrichment analysis tool, KSEA, was used to add another layer to the examination of the Phosphoproteomics data. With this, every known kinase was assigned a z-score, based on how many known (and predicted) substrates of the corresponding kinase were present in the experimental data. The R script written to access KSEA offline is presented in

Supplemental Text *1*. The higher the z-score, the more active a given kinase is in one experimental condition compared to a second condition. The kinase with the highest z-score – in both H358 and H441 – was cyclin-dependent kinase 2, CDK2 (**Figure 15** and **Figure 16**, red bars indicate p-value < 0.05). This kinase is known for phosphorylating β-catenin further hinting to the Wnt pathway being affected by MGL activity. Aside from two other CDKs (CDK1 and CDK7) glycogen synthase kinase-3 beta (GSK3B) was among the highest z-scores

in H358 cells, however reaching no statistical significance. GSK3B is a paralogous protein to GSK3A, which was found in the PHOTON analysis to be less active upon MGL inhibition. While these results contradict each other, PHOTON signaling scores and KSEA z-scores are not directly comparable, with the former looking at the complete known interaction map of proteins based on the experimental results and the latter looking at the presence of peptides known or predicted to be kinase substrates. This little, yet complex discrepancy might be the reason for this seeming contradiction. Furthermore, KSEA found AKT1 to be more active when MGL was inhibited. The z-score for this kinase was not of statistical significance however, with a p-value of around 0.2.

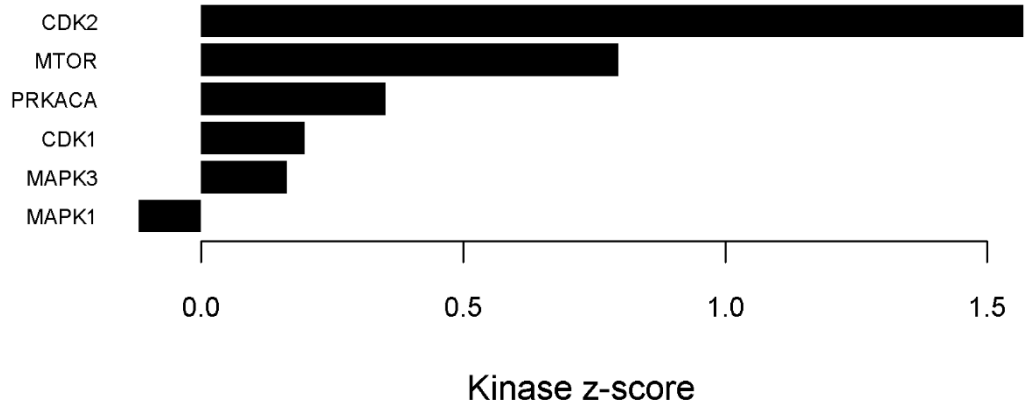

Figure 15: Few kinases were found to be more active in H441 cells upon MGL inhibition. Z-scores are calculated by KSEA based on the number of known and predicted substrates of each kinase found in the dataset and their fold change between the treatment and the control group. A cut-off of 5 substrates was set for kinases to be included in the bar blot.

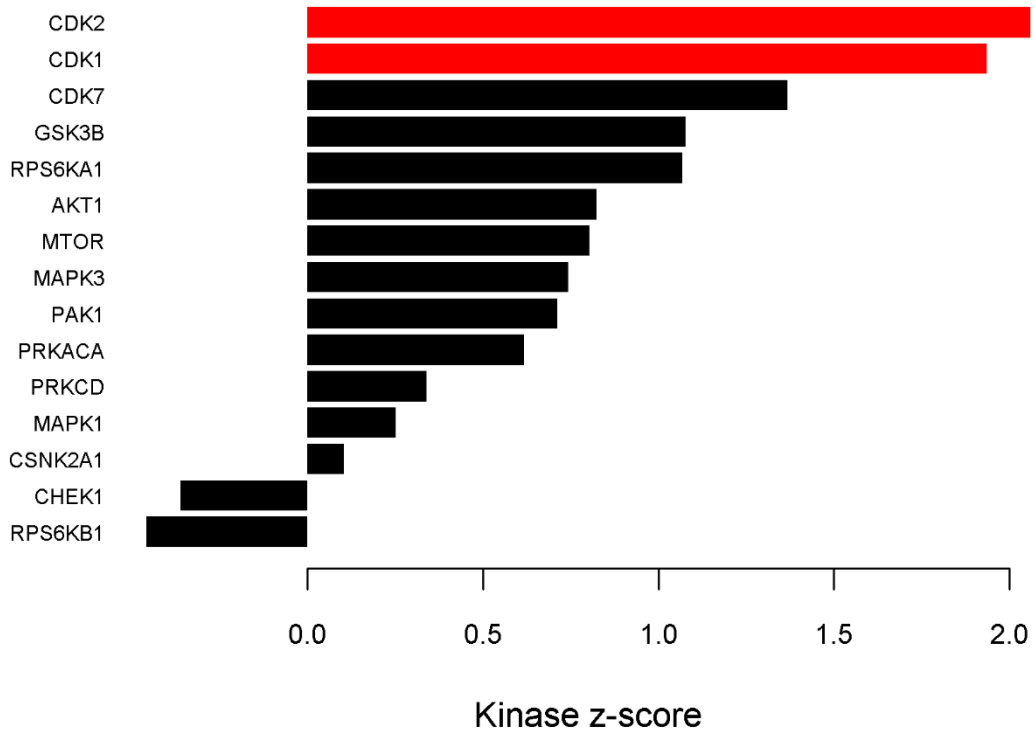

Figure 16: Several kinases were found to be more active in H358 cells upon MGL inhibition. Z-scores are calculated by KSEA based on the number of known and predicted substrates of each kinase found in the dataset and their fold change between the treatment and the control group. A cut-off of 5 substrates was set for kinases to be included in the bar blot. Red bars indicate a p-value < 0.05.

Discussion

The experiments performed in this Master thesis showed, that, in terms of abundance of lipolytic proteins on a protein level, in lipid droplet content and expression levels of some selected signaling kinases, there is a huge variability among cancer cell lines, even of the same tissue, e.g. lung. A high amount of lipid droplets would indicate a high number of LD-associated proteins, but also a low activity of lipases. A549 cells express more ATGL and MGL than the other cell lines in the panel tested and contain a medium LD volume. H1299 and H358 contain considerably more LDs than A549, exhibiting little to no expression of those lipases. Since H1299 and H358 are metastatic cell lines, this result could be indicative of a derailed lipid metabolism being helpful in establishing metastasis. Storage lipids could allow lung tumors to be independent of blood vessels regarding nutrients for energy production and thus enable detachment from the primary tumor and establishment of metastases. On the other hand, the cell line with the lowest storage lipid content measured, A427, was also the cell line with the lowest protein levels of ATGL and MGL alike. Since ATGL is the first enzyme in lipolysis (Zimmermann et al. 2004), initiating the breakdown of neutral lipids in lipid droplets, this suggests perhaps large differences in regulation of ATGL in lung cancer. E.g. CGI-58/ABHD5 is known to activate ATGL, while G0S2 inhibits its function (Lass et al. 2006; Yang et al. 2010). Expression of those two regulators of ATGL could also vary in the lung cancer cell line panel, which should be tested in future experiments.

With cell lines other than A549 having quite low MGL protein levels – A427 and H1299 expressing virtually no MGL – the role the enzyme plays in lung cancer is rather inconclusive. On the one hand, (Nomura et al. 2010) suggested that high MGL expression is linked to aggressive cancers in humans and that MGL inhibition would counteract this aggressiveness. Conversely, R. Liu et al. (2018) found a tumor suppressive characteristic of MGL in a mouse model, suggesting MGL to be critical in preventing tumor development. The results presented here are not conclusive as to whether MGL does influence lung cancer cell growth, may it be positively or negatively. They do suggest however that inhibition of MGL activity affects the growth of some –but not all – cell lines examined. H358 and H441 cells appeared to proliferate faster, as examined by MTT assay. This finding was further corroborated by continuous cell imaging over a prolonged period. Here, 7 spots within each well of a 12-well plate were used to calculate a mean per well. These results supported Liu et al.'s findings that MGL activity somewhat hinders cancer development. It furthermore prompted phosphoproteomic analyses of those two cell lines, to aim to unravel the mechanism behind this apparent growth advantage. Considering the recent increase in use of the MGL inhibitor JZL184 in both cancer (Yin et al. 2020; Marino et al. 2020) and non-cancer (Rodrigues et al. 2020) related research, further observations of the effects of this inhibitor could prove useful in the future.

Immunoblotting could not reveal a link between MGL activity and signaling proteins' activity. Neither did the LC-MS/MS experiment reveal major changes in oncogenic signaling pathways. Given that SRC is a tyrosine kinase and only serine and threonine phosphorylations were measured however, no argument can be made whether direct targets of SRC had an altered phosphorylation profile. Among the significantly more phosphorylated peptides in cells where MGL was inhibited was one belonging to CTNND1, a protein interfacing between Wnt signaling and cell-cell adhesions. Gene Ontology terms regarding Wnt signaling are also enriched in the MGL inhibited cells, for both H358 and H441. This was a first hint, that MGL activity somehow influences the Wnt pathway.

The Wnt signaling pathways involvement in cancer has been extensively studied over the years. Wnt-1 was first described as an oncogene in a murine model as early as the early 1980s by Nusse and Varmus (1982). Since then, several components of the Wnt pathway have been implied to play a role in human tumors. The canonical Wnt pathway (β-catenin dependent) is activated by a Wnt protein binding a Frizzled receptor (along with an LRP co-receptor). This, on the one hand, leads to dissociation of E-cadherin from the LRP receptor and, on the other hand, results in phosphorylation of Dishevelled (Dvl). The dissociation of E-cadherin is a result of the activation of CK1ε (by dephosphorylation), which is associated with E-cadherin and δ-catenin and in turn phosphorylates E-cadherin, leading to its dissociation from LRP and CK1ε/δ-catenin. β-catenin is also associated with E-cadherin, dissociates from phosphorylated E-cadherin as well, however (Casagolda et al. 2010). Dvl is part of the so called "destruction complex" (alongside the proteins APC, Axin, GSK3B and CK1α), which is responsible for leading to proteasomal degradation of β-catenin. β-catenin is phosphorylated at Ser33, Ser37 and Thr41 (and Ser45), with these phosphorylations promoting ubiquitination. Phosphorylation of Dvl destabilizes the "destruction complex". Through both described mechanisms, β-catenin accumulates in the cytosol and ultimately translocates into the nucleus, where it – in tandem members of the TCF/LEF transcription factor family – promotes transcription of Wnt target genes (Duchartre, Kim, and Kahn 2016). A graphical summary of the canonical Wnt pathway and how the proteins discussed below affect it, is provided in **Figure 17**. Wnt target genes include, among others, MYC (He et al. 1998), Cyclin D (Shtutman et al. 1999) and PPAR-δ (He et al. 1999), showing the involvement of Wnt signaling in cell proliferation.

The PHOTON software offered another layer of analysis to the experimental data. With it, every protein is assigned a "signaling score", indicating a higher involvement in signaling mechanisms for positive scores or a lower involvement for negative scores, respectively. This score is calculated using the experimentally measured intensities for all phosphopeptides detected. A network of all known protein-protein interactions is then generated with these "signaling scores". Filtering this global network for proteins that have been annotated with the keyword "Wnt" creates a subnetwork, that was the basis for further discussion. Among the proteins with the highest "signaling scores" were Casein kinase II subunit beta

(CSNK2B/CK2β) and Casein kinase I isoform alpha (CSNK1A1/CK1α). It has been found, that Wnt promotes a metastatic stem-cell like behavior in ovarian tumors. This WNT5A-induced effect was also demonstrated to be blocked upon pharmacological inhibition of casein kinase I (Kotrbová et al. 2020). CSNK1A1 is also known to phosphorylate β-catenin at Ser45 (X. Liu et al. 2020), one of the pivotal residues determining the degradation of β-catenin, thus negatively impacting Wnt signaling. Casein kinase II has been shown to also phosphorylate β-catenin, although at Thr393, which stabilizes and aids in accumulation of β-catenin (Song et al. 2003, 2). These findings somewhat contradict each other. They might however be just two sides of the same feedback coin: The increased stability of β-catenin and the following accumulation would lead to a stark increase in expression of Wnt target genes, especially in different stages of the cell cycle, as it has been shown that CDK2 can fine tune β-catenin by phosphorylating at Ser33, Ser37 and Thr41 (leading to degradation of β-catenin over the course of the cell cycle (Park et al. 2004). To counteract an unnecessary overexpression, a possible response of cells could be to in turn destabilize the co-transcription factor, that is necessary for the transcription in the first place. Zhang et al. (2020) also found, that CSNK2 overexpression decreases stability of Tcf7l1. Tcf7l1 is a co-transcription factor in Wnt signaling. Tcf7l1 alone represses transcription of Wnt target genes, while presence of β-catenin activates the transcription. The higher signaling activity of CSNK2B proposes the idea that in H358 Wnt signaling is suppressed when MGL activity is inhibited.

To add to the hypothesis, that the Wnt pathway responds to inhibiting MGL activity, the kinase-substrate enrichment analysis software (KSEA) showed that based on the phosphopeptides found within the samples measured, cyclin-dependent kinase 2 (CDK2) was significantly more active when MGL was inhibited in the cells. CDK2 has already been shown to phosphorylate β-catenin at Ser33, Ser37 and Thr41 (Park et al. 2004). These residues, when phosphorylated, mark β-catenin for degradation by the destruction complex. This indicates downregulation of the Wnt pathway in the measured samples, as they show a higher activity of CDK2 compared to the control cells. This idea is supported by the findings of Kawakami et al. (2017), who suggest that inhibition of CDK2 has antineoplastic effects in lung cancer. Aside from Wnt-related activities, CDK2 acts to regulate transcription over the course of the cell cycle (Lim and Kaldis 2013). **Figure 18** summarizes changes in protein activity within the Wnt pathway for both H358 and H441 cells in accordance to PHOTON and KSEA results based on measured phosphopeptide intensities.To conclude, our findings suggest that in certain lung cancer cell lines monoglycerol lipase seems to inhibit cell growth. This is supported by the increase in proliferation observed when activity of MGL was chemically inhibited. Further analysis pointed toward the Wnt pathway being influenced upon this inhibition of MGL. Our results suggest an inactivation of the Wnt pathway in H358 and H441 lung cancer cells. Future experiments should be targeted towards validation of Wnt deactivation by MGL inhibition, e.g. by qPCR of known Wnt target genes. Such an inactivation in A549 cells was shown to decrease growth, contrary to what we observed (Wang et al. 2020). On the other hand, overexpression

of miR-27a-3p in Triple-Negative Breast Cancer cells promoted growth via inactivation of Wnt by targeting GSK3B (Wu et al. 2020). These findings do not allow to draw a conclusion that explains the role of Wnt in lung cancer in general. They could, however, relate to the fact, that both H358 and H441 cells carry a mutation in the KRAS protein, a part of the Ras/MAPK pathway (Mitsudomi et al. 1992). This underlines the importance of understanding the entire genetic landscape of any single cancer if one hopes to understand what makes or breaks the respective cancer and to find a therapeutic measure against it.

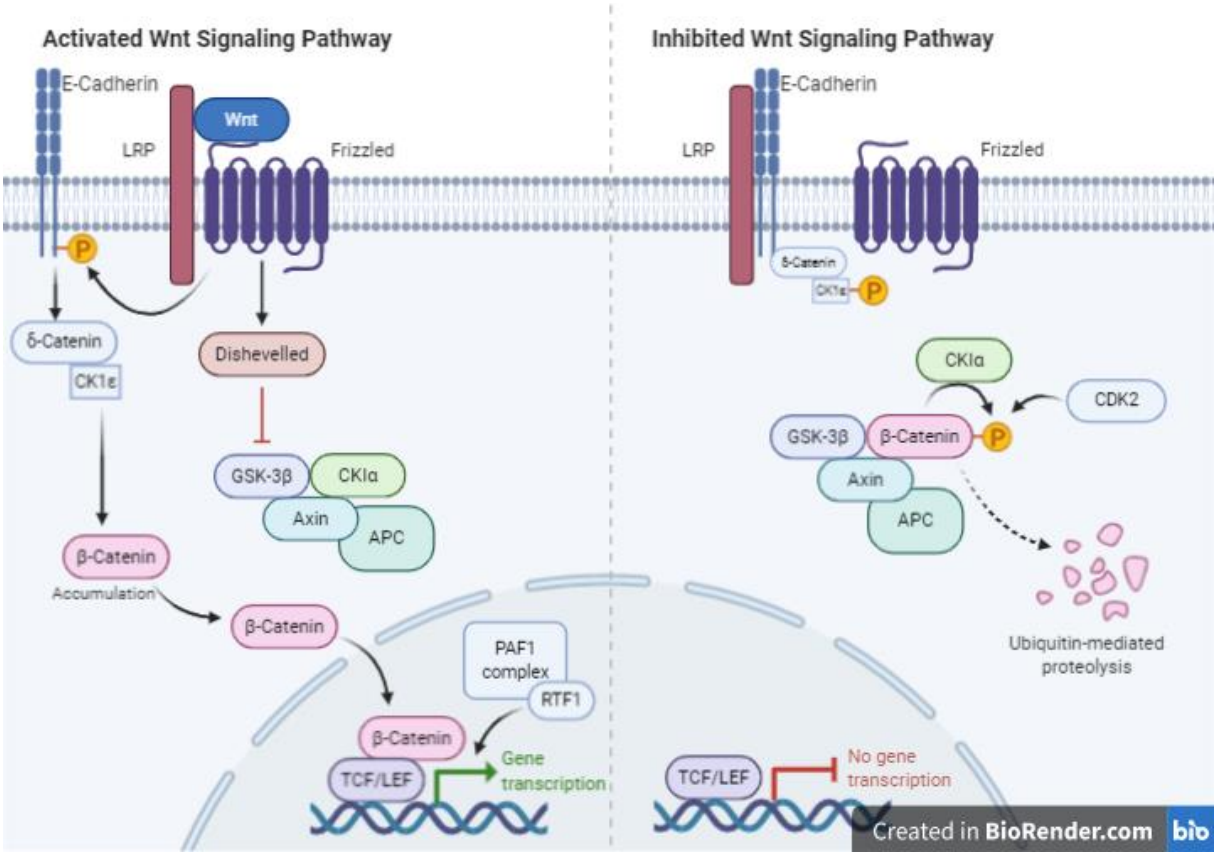

Figure 17: Graphical summary of how different proteins act within the Wnt pathway. When the Wnt pathway is inactive (**right**), E-cadherin is associated with the LRP receptor and δ-catenin and CK1ε are bound to E-cadherin. Furthermore, β-catenin is phosphorylated at specific residues by the "destruction complex", leading to ubiquitination and ultimately to degradation. Upon activation (**left**) of the pathway by binding of a Wnt protein to LRP and Frizzled, E-cadherin is phosphorylated and dissociates from LRP. CK1ε is activated by phosphorylation and dissociated together with δ-catenin from E-cadherin. Also, the Dishevelled protein destabilizes the "destruction complex". These events result in accumulation of β-catenin in the cytosol which then translocates into the nucleus, acting as a co-transcription factor in expression of Wnt target genes.

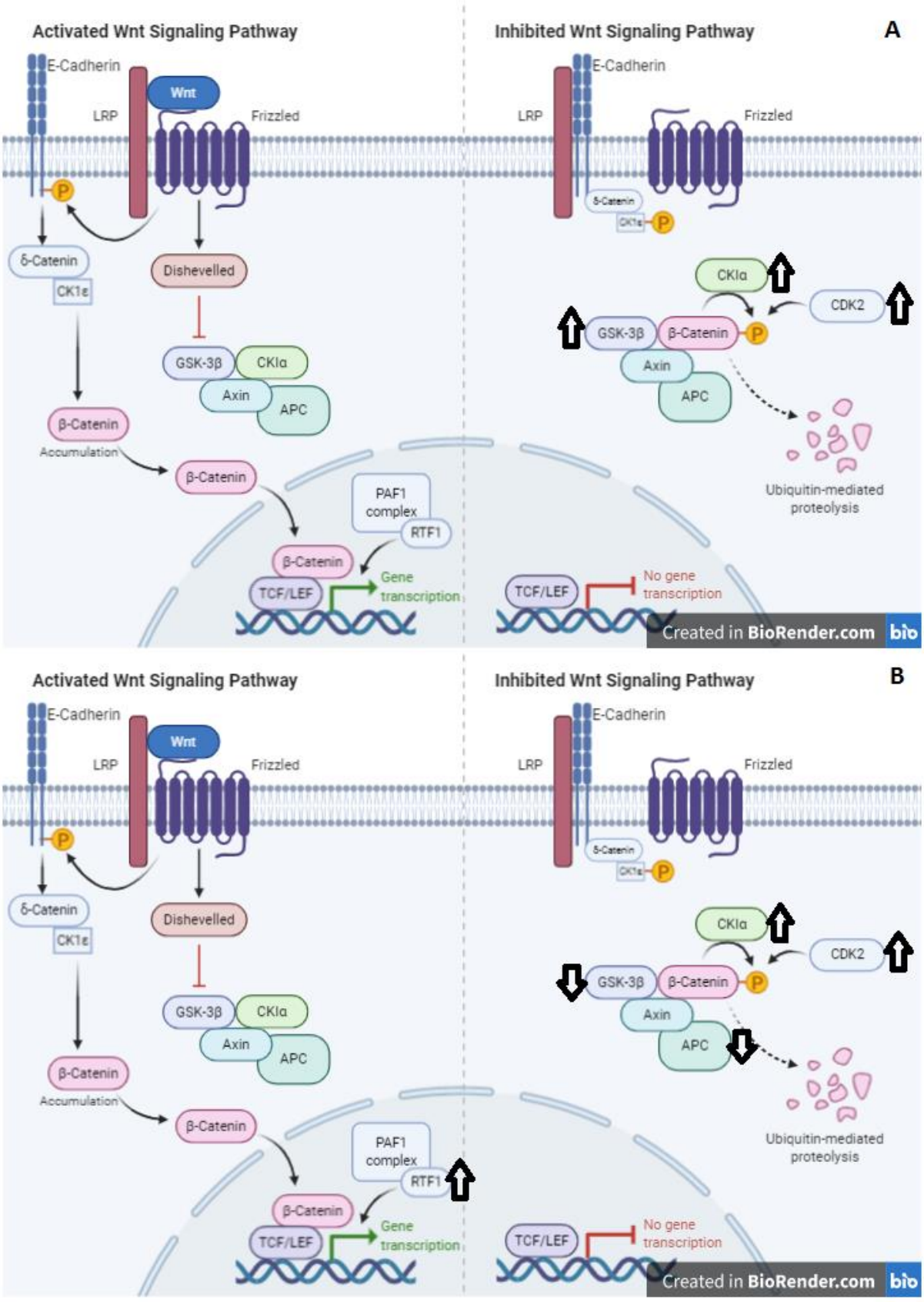

Figure 18: Changes in Wnt signaling pathway observed through changes in phosphoproteome of lung cancer cells. PHOTON and KSEA tools revealed changes (denoted by arrows) in activity of several proteins acting in the Wnt pathway in H358 (A) and H441 (B) cells.

Supplemental Material

Supplemental Table 1: Enriched pathways and GO terms upon inhibition of MGL in H358. Enrichment of KEGG, Reactome and GO terms from top cluster of **Figure 11** based on the total dataset. Enrichment performed in Perseus.

Enriched Term	Enrichment factor	P value	Benj. Hoch. FDR
KEGG			
ko04520: Adherens junction	13.043	2.83E-22	8.98E-20
ko04670: Leukocyte transendothelial migration	10.826	2.62E-12	4.17E-10
Reactome			
REACT_19195: Adherens junctions interactions	12.32	2.84E-13	3.43E-10
REACT_263991: VEGFR2 mediated vascular permeability	11.525	9.08E-13	5.48E-10
GO			
negative regulation of Wnt receptor signaling pathway	15.534	3.64E-15	1.65E-11
negative regulation of canonical Wnt receptor signaling pathway	15.534	3.64E-15	1.65E-11
regulation of canonical Wnt receptor signaling pathway	13.741	3.90E-14	1.18E-10
Wnt receptor signaling pathway	9.8598	5.65E-14	1.28E-10
regulation of Wnt receptor signaling pathway	13.232	7.84E-14	1.42E-10
adherens junction organization	9.9242	1.10E-11	1.66E-08
vascular endothelial growth factor receptor signaling pathway	9.4019	2.62E-11	2.97E-08
cellular response to vascular endothelial growth factor stimulus	9.4019	2.62E-11	2.97E-08
neuron migration	17.667	8.47E-11	6.97E-08
cellular response to growth factor stimulus	6.6743	7.87E-11	6.97E-08
response to growth factor stimulus	6.2874	2.21E-10	1.67E-07
brain development	8.1198	2.55E-10	1.78E-07

Supplemental Table 2: Enriched pathways and GO terms upon inhibition of MGL activity in H441. Enrichment of KEGG, Reactome and GO terms from top cluster of **Figure 12** based on the total dataset. Enrichment performed in Perseus.

Enriched Term	Enrichment factor	P value	Benj. Hoch. FDR
KEGG			
ko04520: Adherens junction	8	1,22E-06	0,00030543
ko04670: Leukocyte transendothelial migration	8,4	2,42E-05	0,0030223
Reactome			
REACT_263991: VEGFR2 mediated vascular permeability	11,455	2,61E-06	0,0010735
REACT_19195: Adherens junctions interactions	11,455	2,61E-06	0,0010735
GO			
vascular endothelial growth factor receptor signaling pathway	12	2.32E-08	7.96E-05
cellular response to vascular endothelial growth factor stimulus	12	2.32E-08	7.96E-05
negative regulation of Wnt receptor signaling pathway	14	5.14E-07	0.00088076
negative regulation of canonical Wnt receptor signaling pathway	14	5.14E-07	0.00088076
regulation of canonical Wnt receptor signaling pathway	11.455	2.61E-06	0.001629
adherens junction organization	10.5	5.02E-06	0.0022972
cellular response to growth factor stimulus	6.4615	7.82E-06	0.0033508
regulation of Wnt receptor signaling pathway	9.6923	8.97E-06	0.0036194
response to growth factor stimulus	6	1.44E-05	0.0048101
anatomical structure development	3.1744	3.17E-05	0.0098891
Wnt receptor signaling pathway	7.875	3.72E-05	0.01063
brain development	7.875	3.72E-05	0.01063
organ development	4.3953	5.76E-05	0.015816

Supplemental Text 1: Code to run KSEA within R.

```
#@@@@@@@@@@@@@@@@@@@@@@@@@@@@@@@@@@@@@@@@@@@@@@@@@@@@@@@@@@@@@@@@@@@@@@@@@@@@@@@@@@@@@@@@@@@@@@@@@@@@@@@@@@@@@@@@@@@@@@@@@@@@@@@@@@@@@@@@@@@@@@@
# Script for KSEA app from Perseus .txt file
#@@@@@@@@@@@@@@@@@@@@@@@@@@@@@@@@@@@@@@@@@@@@@@@@@@@@@@@@@@@@@@@@@@@@@@@@@@@@@@@@@@@@@@@@@@@@@@@@@@@@@@@@@@@@@@@@@@@@@@@@@@@@@@@@@@@@@@@@@@@@@@@@

### set working directory to KSEA_output folder on proteomics drive
### move the files IMMEDIATELLY AFTER!!! Further runs will overwrite the old files otherwise!

getwd()
setwd("R:/KSEA_output")
getwd()

### load the tcltk and KSEA package

library(tcltk)
library(KSEAapp)

### load "KSData" as a dataset for the calculations

load("C:/Program Files/R/R-3.5.1/library/KSEAapp/data/KSData.RData")

### choose .txt file exported form Perseus

#raw_data <- read.delim(file.choose())
raw_data <- read.delim(tk_choose.files(caption = "Select File"))

### remove headers from .txt file

raw_data_formated <- raw_data[-c(1),]

### extract and format required colums

subset_wo_p_FC <- subset(raw_data_formated, select =
c("Protein","Gene.names","Sequence.window","Amino.acid","Position"))
subset_wo_p_FC$Residue.Both <- paste(subset_wo_p_FC$Amino.acid,subset_wo_p_FC$Position)
subset_wo_p_FC$Residue.Both <- gsub('\\s+',", subset_wo_p_FC$Residue.Both)
subset_wo_p_FC <- subset(subset_wo_p_FC, select = -c(Amino.acid,Position))
subsetting <- function(dt) {
  subset(raw_data_formated, select = grep("Student.s.T.test.p.value|_x.y_", names(raw_data_formated)))
}
subset_p_FC <- subsetting(raw_data_formated)
total_subset <- do.call (cbind, list(subset_wo_p_FC,subset_p_FC))

names(total_subset)[2] <- "Gene"
names(total_subset)[3] <- "Peptide"
names(total_subset)[5] <- "p"
names(total_subset)[6] <- "FC"

### OPTIONAL: use to replace "NaN" or blank cells with "NULL" if any cells have missing values

# total_subset[total_subset==""] <- NULL
# total_subset[total_subset=="NaN"] <- NULL

### run KSEA

### here, settings can be changed

### NetworKIN: TRUE or FALSE, TRUE includes NetworKIN predictions in calculation
### NetworKIN.cutoff: minimum NetworKIN score, min. 1 (only necessary if NetworKIN = TRUE)
### m.cutoff: minimum # of substrates of a kinase to be in dataset to include kinase in bar plot, min. 0
### p.cutoff: p-value cutoff for significance in bar plot, between 0 and 1

KSEAapp::KSEA.Complete(KSData, total_subset, NetworKIN = TRUE,
                NetworKIN.cutoff = 5, m.cutoff = 5, p.cutoff = 0.05)
```

References

Anastas, Jamie N., and Randall T. Moon. 2013. "WNT Signalling Pathways as Therapeutic Targets in Cancer." *Nature Reviews Cancer* 13 (1): 11–26. https://doi.org/10.1038/nrc3419.

Beloribi-Djefaflia, S, S Vasseur, and F Guillaumond. 2016. "Lipid Metabolic Reprogramming in Cancer Cells." *Oncogenesis* 5 (1): e189. https://doi.org/10.1038/oncsis.2015.49.

Bodner, S. M., J. D. Minna, S. M. Jensen, D. D'Amico, D. Carbone, T. Mitsudomi, J. Fedorko, D. L. Buchhagen, M. M. Nau, and A. F. Gazdar. 1992. "Expression of Mutant P53 Proteins in Lung Cancer Correlates with the Class of P53 Gene Mutation." *Oncogene* 7 (4): 743–49.

Casagolda, David, Beatriz del Valle-Pérez, Gabriela Valls, Ero Lugilde, Meritxell Vinyoles, Juan Casado-Vela, Guiomar Solanas, et al. 2010. "A P120-Catenin–CK1ε Complex Regulates Wnt Signaling." *Journal of Cell Science* 123 (15): 2621–31. https://doi.org/10.1242/jcs.067512.

Cox, Jürgen, and Matthias Mann. 2008. "MaxQuant Enables High Peptide Identification Rates, Individualized p.p.b.-Range Mass Accuracies and Proteome-Wide Protein Quantification." *Nature Biotechnology* 26 (12): 1367–72. https://doi.org/10.1038/nbt.1511.

Cruz, André L. S., Ester de A. Barreto, Narayana P. B. Fazolini, João P. B. Viola, and Patricia T. Bozza. 2020. "Lipid Droplets: Platforms with Multiple Functions in Cancer Hallmarks." *Cell Death & Disease* 11 (2). https://doi.org/10.1038/s41419-020-2297-3.

David, Odile, James Jett, Helena LeBeau, Grace Dy, Janet Hughes, Mitchell Friedman, and Arnold R. Brody. 2004. "Phospho-Akt Overexpression in Non–Small Cell Lung Cancer Confers Significant Stage-Independent Survival Disadvantage." *Clinical Cancer Research* 10 (20): 6865–71. https://doi.org/10.1158/1078-0432.CCR-04-0174.

Di Leo, Luca, Rolando Vegliante, Fabio Ciccarone, Illari Salvatori, Manuel Scimeca, Elena Bonanno, Andrea Sagnotta, Gian Luca Grazi, Katia Aquilano, and Maria Rosa Ciriolo. 2019. "Forcing ATGL Expression in Hepatocarcinoma Cells Imposes Glycolytic Rewiring through PPAR-α/P300-Mediated Acetylation of P53." *Oncogene* 38 (11): 1860–75. https://doi.org/10.1038/s41388-018-0545-0.

Du, Lei, Yu-Hong Yang, Yu-Ming Wang, Chang-Hu Xue, Hideyuki Kurihara, and Koretaro Takahashi. 2015. "EPA-Enriched Phospholipids Ameliorate Cancer-Associated Cachexia Mainly via Inhibiting Lipolysis." *Food & Function* 6 (12): 3652–62. https://doi.org/10.1039/c5fo00478k.

Duchartre, Yann, Yong-Mi Kim, and Michael Kahn. 2016. "The Wnt Signaling Pathway in Cancer." *Critical Reviews in Oncology/Hematology* 99 (March): 141–49. https://doi.org/10.1016/j.critrevonc.2015.12.005.

Ferlay, J., M. Colombet, I. Soerjomataram, T. Dyba, G. Randi, M. Bettio, A. Gavin, O. Visser, and F. Bray. 2018. "Cancer Incidence and Mortality Patterns in Europe: Estimates for 40 Countries and 25 Major Cancers in 2018." *European Journal of Cancer* 103 (November): 356–87. https://doi.org/10.1016/j.ejca.2018.07.005.

Giaccone, G., and P. A. Zucali. 2008. "Src as a Potential Therapeutic Target in Non-Small-Cell Lung Cancer." *Annals of Oncology* 19 (7): 1219–23. https://doi.org/10.1093/annonc/mdn048.

He, T. C., T. A. Chan, B. Vogelstein, and K. W. Kinzler. 1999. "PPARdelta Is an APC-Regulated Target of Nonsteroidal Anti-Inflammatory Drugs." *Cell* 99 (3): 335–45. https://doi.org/10.1016/s0092-8674(00)81664-5.

He, T. C., A. B. Sparks, C. Rago, H. Hermeking, L. Zawel, L. T. da Costa, P. J. Morin, B. Vogelstein, and K. W. Kinzler. 1998. “Identification of C-MYC as a Target of the APC Pathway.” *Science (New York, N.Y.)* 281 (5382): 1509–12. https://doi.org/10.1126/science.281.5382.1509.

Hornbeck, Peter V., Bin Zhang, Beth Murray, Jon M. Kornhauser, Vaughan Latham, and Elzbieta Skrzypek. 2015. “PhosphoSitePlus, 2014: Mutations, PTMs and Recalibrations.” *Nucleic Acids Research* 43 (Database issue): D512-520. https://doi.org/10.1093/nar/gku1267.

Humphrey, Sean J., S. Babak Azimifar, and Matthias Mann. 2015. “High-Throughput Phosphoproteomics Reveals in Vivo Insulin Signaling Dynamics.” *Nature Biotechnology* 33 (9): 990–95. https://doi.org/10.1038/nbt.3327.

Humphries, Ashley Ceinwen, and Marek Mlodzik. 2018. “From Instruction to Output: Wnt/PCP Signaling in Development and Cancer.” *Current Opinion in Cell Biology* 51 (April): 110–16. https://doi.org/10.1016/j.ceb.2017.12.005.

Kawakami, Masanori, Lisa Maria Mustachio, Jaime Rodriguez-Canales, Barbara Mino, Jason Roszik, Pan Tong, Jing Wang, et al. 2017. “Next-Generation CDK2/9 Inhibitors and Anaphase Catastrophe in Lung Cancer.” *Journal of the National Cancer Institute* 109 (6). https://doi.org/10.1093/jnci/djw297.

Knapp, M., and J. Gorski. 2017. “The Skeletal and Heart Muscle Triacylglycerol Lipolysis Revisited.” *Journal of Physiology and Pharmacology: An Official Journal of the Polish Physiological Society* 68 (1): 3–11.

Kotrbová, Anna, Petra Ovesná, Tomáš Gybel’, Tomasz Radaszkiewicz, Markéta Bednaříková, Jitka Hausnerová, Eva Jandáková, et al. 2020. “WNT Signaling Inducing Activity in Ascites Predicts Poor Outcome in Ovarian Cancer.” *Theranostics* 10 (2): 537–52. https://doi.org/10.7150/thno.37423.

Lass, Achim, Robert Zimmermann, Guenter Haemmerle, Monika Riederer, Gabriele Schoiswohl, Martina Schweiger, Petra Kienesberger, Juliane G. Strauss, Gregor Gorkiewicz, and Rudolf Zechner. 2006. “Adipose Triglyceride Lipase-Mediated Lipolysis of Cellular Fat Stores Is Activated by CGI-58 and Defective in Chanarin-Dorfman Syndrome.” *Cell Metabolism* 3 (5): 309–19. https://doi.org/10.1016/j.cmet.2006.03.005.

Lim, Shuhui, and Philipp Kaldis. 2013. “Cdks, Cyclins and CKIs: Roles beyond Cell Cycle Regulation.” *Development* 140 (15): 3079–93. https://doi.org/10.1242/dev.091744.

Liu, Renyan, Xin Wang, Christopher Curtiss, Steve Landas, Rong Rong, M. Saeed Sheikh, and Ying Huang. 2018. “Monoglyceride Lipase Gene Knockout in Mice Leads to Increased Incidence of Lung Adenocarcinoma.” *Cell Death & Disease* 9 (2). https://doi.org/10.1038/s41419-017-0188-z.

Liu, Xia, Qingling Huang, Lihong Chen, Huilai Zhang, Ernst Schonbrunn, and Jiandong Chen. 2020. “Tumor-Derived CK1α Mutations Enhance MDMX Inhibition of P53.” *Oncogene* 39 (1): 176–86. https://doi.org/10.1038/s41388-019-0979-z.

Marino, Silvia, Giovana Carrasco, Boya Li, Karan M. Shah, Darren L. Lath, Antonia Sophocleous, Michelle A. Lawson, and Aymen I. Idris. 2020. “JZL184, A Monoacylglycerol Lipase Inhibitor, Induces Bone Loss in a Multiple Myeloma Model of Immunocompetent Mice.” *Calcified Tissue International* 107 (1): 72–85. https://doi.org/10.1007/s00223-020-00689-0.

Menendez, Javier A. 2010. “Fine-Tuning the Lipogenic/Lipolytic Balance to Optimize the Metabolic Requirements of Cancer Cell Growth: Molecular Mechanisms and Therapeutic Perspectives.” *Biochimica Et Biophysica Acta* 1801 (3): 381–91. https://doi.org/10.1016/j.bbalip.2009.09.005.

Mitsudomi, T., S. M. Steinberg, M. M. Nau, D. Carbone, D. D’Amico, S. Bodner, H. K. Oie, R. I. Linnoila, J. L. Mulshine, and J. D. Minna. 1992. “P53 Gene Mutations in Non-

Small-Cell Lung Cancer Cell Lines and Their Correlation with the Presence of Ras Mutations and Clinical Features." *Oncogene* 7 (1): 171–80.

Molendijk, J., H. Robinson, Z. Djuric, and M. M. Hill. 2020. "Lipid Mechanisms in Hallmarks of Cancer." *Molecular Omics* 16 (1): 6–18. https://doi.org/10.1039/C9MO00128J.

Nomura, Daniel K., Jonathan Z. Long, Sherry Niessen, Heather S. Hoover, Shu-Wing Ng, and Benjamin F. Cravatt. 2010. "Monoacylglycerol Lipase Regulates a Fatty Acid Network That Promotes Cancer Pathogenesis." *Cell* 140 (1): 49–61. https://doi.org/10.1016/j.cell.2009.11.027.

Nusse, R., and H. E. Varmus. 1982. "Many Tumors Induced by the Mouse Mammary Tumor Virus Contain a Provirus Integrated in the Same Region of the Host Genome." *Cell* 31 (1): 99–109. https://doi.org/10.1016/0092-8674(82)90409-3.

Park, Chun Shik, Sung Il Kim, Mi Su Lee, Cho-Ya Youn, Dae Joong Kim, Eek-Hoon Jho, and Woo Keun Song. 2004. "Modulation of Beta-Catenin Phosphorylation/Degradation by Cyclin-Dependent Kinase 2." *The Journal of Biological Chemistry* 279 (19): 19592–99. https://doi.org/10.1074/jbc.M314208200.

Rapp, Judit, Luca Jaromi, Krisztian Kvell, Gyorgy Miskei, and Judit E. Pongracz. 2017. "WNT Signaling – Lung Cancer Is No Exception." *Respiratory Research* 18. https://doi.org/10.1186/s12931-017-0650-6.

Raslan, Ahmed A., and Jeong Kyo Yoon. 2020. "WNT Signaling in Lung Repair and Regeneration." *Molecules and Cells*, August. https://doi.org/10.14348/molcells.2020.0059.

Rodrigues, Matilde S., Cláudia Ferreira, Cândida Dias, Anna Pliássova, Lisiane Souza, Ana Ledo, João Laranjinha, Rodrigo A. Cunha, and Attila Köfalvi. 2020. "An Optimized Spectrophotometric Assay Reveals Increased Activity of Enzymes Involved in 2-Arachidonoyl Glycerol Turnover in the Cerebral Cortex of a Rat Model of Alzheimer's Disease." *The European Journal of Neuroscience*, August. https://doi.org/10.1111/ejn.14944.

Rudolph, Jan Daniel, Marjo de Graauw, Bob van de Water, Tamar Geiger, and Roded Sharan. 2016. "Elucidation of Signaling Pathways from Large-Scale Phosphoproteomic Data Using Protein Interaction Networks." *Cell Systems* 3 (6): 585-593.e3. https://doi.org/10.1016/j.cels.2016.11.005.

Shannon, Paul, Andrew Markiel, Owen Ozier, Nitin S. Baliga, Jonathan T. Wang, Daniel Ramage, Nada Amin, Benno Schwikowski, and Trey Ideker. 2003. "Cytoscape: A Software Environment for Integrated Models of Biomolecular Interaction Networks." *Genome Research* 13 (11): 2498–2504. https://doi.org/10.1101/gr.1239303.

Shtutman, M., J. Zhurinsky, I. Simcha, C. Albanese, M. D'Amico, R. Pestell, and A. Ben-Ze'ev. 1999. "The Cyclin D1 Gene Is a Target of the Beta-Catenin/LEF-1 Pathway." *Proceedings of the National Academy of Sciences of the United States of America* 96 (10): 5522–27. https://doi.org/10.1073/pnas.96.10.5522.

Siegel, Rebecca L., Kimberly D. Miller, and Ahmedin Jemal. 2020. "Cancer Statistics, 2020." *CA: A Cancer Journal for Clinicians* 70 (1): 7–30. https://doi.org/10.3322/caac.21590.

Sigismund, Sara, Daniele Avanzato, and Letizia Lanzetti. 2018. "Emerging Functions of the EGFR in Cancer." *Molecular Oncology* 12 (1): 3–20. https://doi.org/10.1002/1878-0261.12155.

Song, Diane H., Isabel Dominguez, Junko Mizuno, Maurya Kaut, Scott C. Mohr, and David C. Seldin. 2003. "CK2 Phosphorylation of the Armadillo Repeat Region of Beta-Catenin Potentiates Wnt Signaling." *The Journal of Biological Chemistry* 278 (26): 24018–25. https://doi.org/10.1074/jbc.M212260200.

Sun, Hong, Lingyan Jiang, Xiuquan Luo, Weixin Jin, Qin He, Jie An, Ki Lui, et al. 2013. "Potential Tumor Suppressive Role of Monoglyceride Lipase in Human Colorectal Cancer." *Oncogene* 32 (2): 234–41. https://doi.org/10.1038/onc.2012.34.

Szklarczyk, Damian, Annika L. Gable, David Lyon, Alexander Junge, Stefan Wyder, Jaime Huerta-Cepas, Milan Simonovic, et al. 2019. "STRING V11: Protein-Protein Association Networks with Increased Coverage, Supporting Functional Discovery in Genome-Wide Experimental Datasets." *Nucleic Acids Research* 47 (D1): D607–13. https://doi.org/10.1093/nar/gky1131.

Tomin, Tamara, Katarina Fritz, Juergen Gindlhuber, Linda Waldherr, Bettina Pucher, Gerhard G. Thallinger, Daniel K. Nomura, Matthias Schittmayer, and Ruth Birner-Gruenberger. 2018. "Deletion of Adipose Triglyceride Lipase Links Triacylglycerol Accumulation to a More-Aggressive Phenotype in A549 Lung Carcinoma Cells." *Journal of Proteome Research* 17 (4): 1415–25. https://doi.org/10.1021/acs.jproteome.7b00782.

Tyanova, Stefka, Tikira Temu, Pavel Sinitcyn, Arthur Carlson, Marco Y. Hein, Tamar Geiger, Matthias Mann, and Jürgen Cox. 2016. "The Perseus Computational Platform for Comprehensive Analysis of (Prote)Omics Data." *Nature Methods* 13 (9): 731–40. https://doi.org/10.1038/nmeth.3901.

Vicent, S, J M López-Picazo, G Toledo, M D Lozano, W Torre, C Garcia-Corchón, C Quero, et al. 2004. "ERK1/2 Is Activated in Non-Small-Cell Lung Cancer and Associated with Advanced Tumours." *British Journal of Cancer* 90 (5): 1047–52. https://doi.org/10.1038/sj.bjc.6601644.

Wang, Xiao-Hui, Shu-Ying Zhang, Mei Shi, and Xiao-Peng Xu. 2020. "HMGB1 Promotes the Proliferation and Metastasis of Lung Cancer by Activating the Wnt/β-Catenin Pathway." *Technology in Cancer Research & Treatment* 19 (December): 1533033820948054. https://doi.org/10.1177/1533033820948054.

Warburg, Otto, Franz Wind, and Erwin Negelein. 1926. "Über den Stoffwechsel von Tumoren im Körper." *Klinische Wochenschrift* 5 (19): 829–32. https://doi.org/10.1007/BF01726240.

Wiredja, Danica D., Mehmet Koyutürk, and Mark R. Chance. 2017. "The KSEA App: A Web-Based Tool for Kinase Activity Inference from Quantitative Phosphoproteomics." *Bioinformatics (Oxford, England)* 33 (21): 3489–91. https://doi.org/10.1093/bioinformatics/btx415.

Wu, Ruizhen, Bingqing Zhao, Xunxin Ren, Shiheng Wu, Mingzao Liu, Zipeng Wang, and Wei Liu. 2020. "MiR-27a-3p Targeting GSK3β Promotes Triple-Negative Breast Cancer Proliferation and Migration Through Wnt/β-Catenin Pathway." *Cancer Management and Research* 12 (July): 6241–49. https://doi.org/10.2147/CMAR.S255419.

Yang, Xingyuan, Xin Lu, Marc Lombès, Geun Bae Rha, Young-In Chi, Theresa M. Guerin, Eric J. Smart, and Jun Liu. 2010. "The G0/G1 Switch Gene 2 Regulates Adipose Lipolysis through Association with Adipose Triglyceride Lipase." *Cell Metabolism* 11 (3): 194–205. https://doi.org/10.1016/j.cmet.2010.02.003.

Yin, Jinlong, Sung Soo Kim, Eunji Choi, Young Taek Oh, Weiwei Lin, Tae-Hoon Kim, Jason K. Sa, et al. 2020. "ARS2/MAGL Signaling in Glioblastoma Stem Cells Promotes Self-Renewal and M2-like Polarization of Tumor-Associated Macrophages." *Nature Communications* 11 (1): 2978. https://doi.org/10.1038/s41467-020-16789-2.

Zhang, Yan, Zhenhua Zhu, Huiwen Ding, Shengpeng Wan, Xinbao Zhang, Yuting Li, Junxiang Ji, Xin Wang, Meng Zhang, and Shou-Dong Ye. 2020. "β-Catenin Stimulates Tcf7l1 Degradation through Recruitment of Casein Kinase 2 in Mouse Embryonic Stem Cells." *Biochemical and Biophysical Research Communications* 524 (2): 280–87. https://doi.org/10.1016/j.bbrc.2020.01.074.

Zimmermann, Robert, Juliane G. Strauss, Guenter Haemmerle, Gabriele Schoiswohl, Ruth Birner-Gruenberger, Monika Riederer, Achim Lass, et al. 2004. "Fat Mobilization in Adipose Tissue Is Promoted by Adipose Triglyceride Lipase." *Science* 306 (5700): 1383–86. https://doi.org/10.1126/science.1100747.